iScience

CellPress
OPEN ACCESS

Article

Single-nucleus chromatin accessibility and RNA sequencing reveal impaired brain development in prenatally e-cigarette exposed neonatal rats

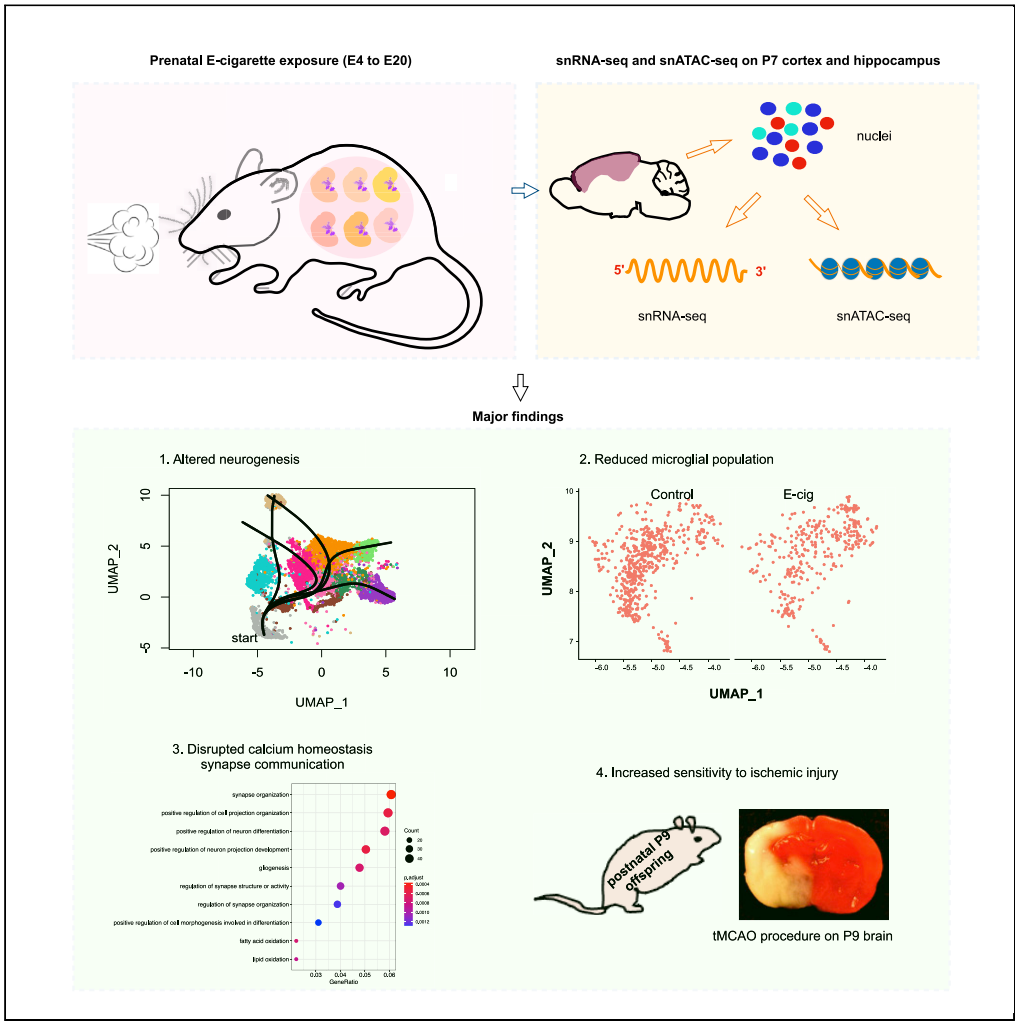

Zhong Chen, Wanqiu Chen, Yong Li, Malcolm Moos, Jr., Daliao Xiao, Charles Wang

dxiao@llu.edu (D.X.)
chwang@llu.edu (C.W.)

Highlights

Prenatal e-cigarette exposure adversely affects rat brain development

Prenatal e-cigarette smoking disrupts brain excitatory/inhibitory neuron balance

Prenatal e-cigarette smoking disrupts Ca^{2+} homeostasis, induces microglia cell death

Prenatal e-cigarette exposure increases susceptibility to brain ischemic injury

Chen et al., iScience *25*, 104686
August 19, 2022
https://doi.org/10.1016/j.isci.2022.104686

iScience

CellPress
OPEN ACCESS

Article

Single-nucleus chromatin accessibility and RNA sequencing reveal impaired brain development in prenatally e-cigarette exposed neonatal rats

Zhong Chen,[1,5] Wanqiu Chen,[1,5] Yong Li,[2,5] Malcolm Moos, Jr.,[3] Daliao Xiao,[2,*] and Charles Wang[1,4,6,*]

SUMMARY

Although emerging evidence reveals that vaping alters the function of the central nervous system, the effects of maternal vaping on offspring brain development remain elusive. Using a well-established *in utero* exposure model, we performed single-nucleus ATAC-seq (snATAC-seq) and RNA sequencing (snRNA-seq) on prenatally e-cigarette-exposed rat brains. We found that maternal vaping distorted neuronal lineage differentiation in the neonatal brain by promoting excitatory neurons and inhibiting lateral ganglionic eminence-derived inhibitory neuronal differentiation. Moreover, maternal vaping disrupted calcium homeostasis, induced microglia cell death, and elevated susceptibility to cerebral ischemic injury in the developing brain of offspring. Our results suggest that the aberrant calcium signaling, diminished microglial population, and impaired microglia-neuron interaction may all contribute to the underlying mechanisms by which prenatal e-cigarette exposure impairs neonatal rat brain development. Our findings raise the concern that maternal vaping may cause adverse long-term brain damage to the offspring.

INTRODUCTION

Maternal smoking is a well-recognized public health concern associated with increased health risks in offspring (Alkam et al., 2013; Visser et al., 2019). In addition to increased perinatal mortality and morbidity and other severe obstetric complications, substantial evidence reveals various adverse effects of maternal cigarette smoking, especially on brain development (Li et al., 2012; Ruszkiewicz et al., 2020; Sailer et al., 2019; Schmidt, 2020; Zelikoff et al., 2018). Numerous studies have already documented diverse long-term negative neuropsychiatric effects of prenatal/perinatal nicotine exposure in rodent offspring, such as hyperactivity, reduced cognitive performance, increased anxiety and depression, and enhanced vulnerability to brain hypoxia-ischemia (HI) challenge, etc. (Alkam et al., 2013; Lacy et al., 2016; Lee et al., 2016; Li et al., 2012, 2013; Newman et al., 1999; Pinheiro et al., 2015; Zhang et al., 2018, 2019).

Electronic cigarettes (E-cigarettes) serve as battery-powered nicotine delivery systems (ENDS), which came into the US market in 2007 (Ruszkiewicz et al., 2020), proposed both for recreation and as an aid to smoking cessation. Commonly being perceived as a safer alternative to conventional combustible smoking because of their reportedly lower levels of nicotine and other toxic chemicals (Baeza-Loya et al., 2014; McCubbin et al., 2017; Whittington et al., 2018), ENDS have become popular in the general population, especially in pregnant women and adolescents (Ruszkiewicz et al., 2020; Schmidt, 2020). A recent survey reported that up to 15% of pregnant women in the United States were using E-cigarettes (Whittington et al., 2018). However, emerging evidence suggests potential health risks for ENDS. Compared with conventional combustible cigarette smoking, ENDS contain other unique constituents beyond nicotine, such as propylene glycol (PG), vegetable glycerin (VG), formaldehyde, acrolein, flavoring chemicals, and other trace elements, some of which may be neurotoxic to the developing fetus and offspring (Ruszkiewicz et al., 2020). Long-term effects of maternal e-cigarette exposure on brain development in offspring are not well defined; however, increasing evidence from animal models suggests that such effects may also be of concern. Recent rodent studies reported that maternal e-cigarette exposure may induce aberrant genetic and/or epigenetic changes in the developing brain (Lauterstein et al., 2016), disruption of normal cortical neuronal morphology and connectivity, disturbance of vital neurotransmitter circuits and brain cytokine signaling, enhanced oxidative stress, abnormal neuroinflammation, and impaired autophagy as well as other aspects

[1]Center for Genomics, School of Medicine, Loma Linda University, 11021 Campus St., Loma Linda, CA 92350, USA

[2]Lawrence D. Longo, MD Center for Perinatal Biology, Division of Pharmacology, Department of Basic Sciences, Loma Linda University School of Medicine, Loma Linda, CA 92350, USA

[3]Center for Biologics Evaluation and Research & Division of Cellular and Gene Therapies, U.S. Food and Drug Administration, 10903 New Hampshire Avenue, Silver Spring, MD 20993, USA

[4]Division of Microbiology & Molecular Genetics, Department of Basic Science, School of Medicine, Loma Linda University, 11021 Campus St., Loma Linda, CA 92350, USA

[5]These authors contributed equally

[6]Lead contact

*Correspondence: dxiao@llu.edu (D.X.), chwang@llu.edu (C.W.)

https://doi.org/10.1016/j.isci.2022.104686

of the immune response (Chen et al., 2018a, 2018b; Dwyer et al., 2009; Hosseinzadeh et al., 2016; Mittleman et al., 1997; Muhammad et al., 2012; Ruszkiewicz et al., 2020; Siniscalco et al., 2018; Smith et al., 2010). Even in the absence of nicotine, ENDS usage during pregnancy is also likely deleterious to the fetus (Church et al., 2020; Ruszkiewicz et al., 2020). Given the rapidly growing popularity of ENDS in pregnant women and their potential detrimental effects on the fetus and offspring, it is urgent to understand the effects of maternal e-cigarette exposure on brain development in detail and decipher the underlying mechanisms of these processes at an advanced molecular and cellular level.

The brain is the most complex organ known, with unmatched cellular heterogeneity and functional complexity. Previous transcriptomic studies evaluating the influence of nicotine exposure used aggregated RNA from brain tissue containing diverse cell types (Lauterstein et al., 2016; Silva et al., 2018; Casserly et al., 2020). This experimental design might mask major changes in specific cell populations due to dilution effects. Single-cell RNA sequencing (scRNA-seq) provides a powerful method to study the transcriptome at single-cell resolution, allowing for characterization of various neuronal and non-neuronal cell types, identification of cell type specific transcriptomic changes, and projection of neuronal development (Lake et al., 2016; Artegiani et al., 2017; Chen et al., 2017). Many brain-associated diseases and degenerative changes associated with aging have been shown to manifest as cell type specific pathophysiology (Mathys et al., 2019; Ximerakis et al., 2019a; Smajić et al., 2020). For example, scRNA-seq revealed that oligodendrocytes, instead of neurons, exhibit the most robust morphine-dependent responses, hinting that more detailed evaluation of myelination defects may contribute novel mechanistic insights into the understanding of opioid addiction (Avey et al., 2018).

Accessibility of different promoters, enhancers, and other cis elements imposes important control over the transcriptome. Measurements of chromatin state using the assay for transposase-accessible chromatin at single-cell level (scATAC-seq) have made tremendous progress in recent years (Sinha et al., 2021). scATAC-seq reveals the progression of epigenetic landscape changes during cell differentiation at bifurcation points and helps provide insights into a cell's past (lineage) and future (terminal fate), which cannot be ascertained by transcriptome assay alone. Integration of scRNA-seq and scATAC-seq data can aid in revealing regulatory elements with respect to specific cell populations, providing deeper understanding of the complex biological process in the brain (Lake et al., 2018).

Here, we performed single nucleus RNA sequencing (snRNA-seq) on over 54,000 cells and single nucleus ATAC sequencing (snATAC-seq) on more than 30,000 cells from the brains of postnatal day 7 (P7) rats that were exposed to e-cigarettes during gestational day 4 (E4) to E20. We found that prenatal e-cigarette exposure caused aberrant neuron differentiation particularly resulting in an increased excitatory neuronal composition and loss of lateral ganglionic eminence (LGE)-derived inhibitory neurons, disrupted calcium signaling in the brain cells, markedly diminished numbers of microglia, and elevated susceptibility to cerebral ischemic injury in the prenatal e-cigarette exposed neonate offspring brain. Overall, this study provides valuable insights into the effects of e-cigarettes on early central nervous system development.

RESULTS

Study design and data generation

Figure 1A illustrates the overall study design. We exposed pregnant rats to either e-cigarette vapor or control air from E4 to E20 and harvested the brains from postnatal day 7 (P7) offspring. The neocortex and hippocampus were dissected from four animals of the same gender and under the same conditions as for nucleus isolation (16 pups derived from 4 dams in total) and pooled. Four single-nucleus RNA-seq (snRNA-seq) libraries and four single-nucleus ATAC-seq (snATAC-seq) libraries (female control, female e-cig, male control, and male e-cig) were generated using 10x Genomics Droplet technology. Herein, the term "rat brain" denotes the combined neocortex and hippocampus tissue only, instead of the whole brain.

In the snRNA-seq experiment, we obtained over 54,000 single-nucleus transcriptomes derived from the P7 brains of eight control (three males and five females) and eight (four males and four females) prenatally e-cigarette exposed rat pups from four separate snRNA-seq libraries. These nuclei were sequenced to an average depth of ~19,000 reads/nucleus with a median UMI count of 2,429. Over 84% of all reads were mapped to the Rn6.0 genome and more than 56% were mapped to exons of the premature RNA reference, with an average of 1,503 genes/nucleus (Table S1). The R package Seurat (v. 3.2.2) was used for downstream analysis. The datasets generated from the four snRNA-seq libraries had similar features and were

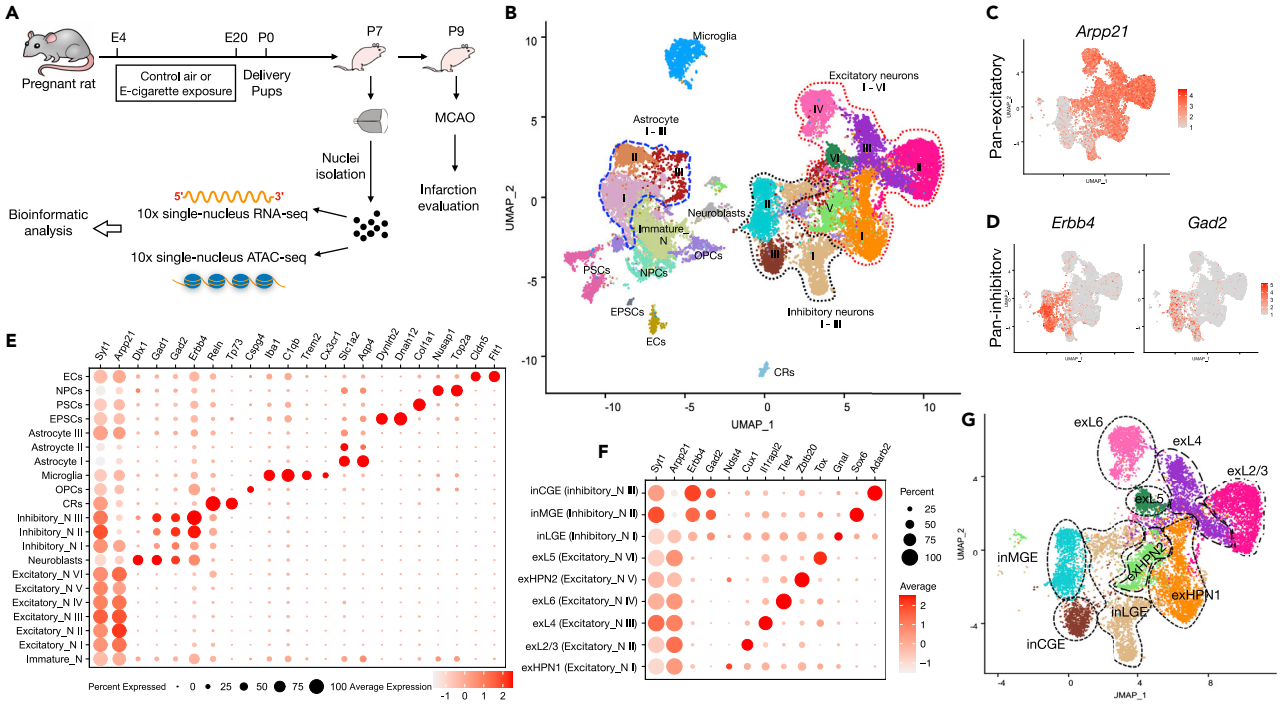

Figure 1. Study design and cell type identification in the neonatal rat brain exposed to prenatal e-cigarette vapor

(A) Overview of study design. Pregnant Sprague-Dawley rats were exposed to control air or e-cigarette from gestational E4 to E20. The brains of postnatal day 7 (P7) rat pups were dissociated to obtain single nuclei for snRNA-seq and snATAC-seq. In some parallel animals, transient middle cerebral artery occlusion (tMCAO) was conducted on postnatal day 9 (P9) rat pups, and the infarct size was evaluated 48h later.

(B) UMAP visualization of 29,317 single nucleus transcriptomes from postnatal day 7 rat brain revealed 21 groups colored by annotated cell type. OPCs, oligodendrocyte progenitor cells; NPCs, neural progenitor cells; PSCs, perivascular stromal cells; EPSCs, ependymal cells; ECs, endothelial cells; CRs, Cajal-Retzius cells.

(C) UMAP visualization of nine neuronal cell populations showing the expression of the representative excitatory neuron marker *Arpp21* and (D). inhibitory neuronal markers *Erbb4* and *Gad2*.

(E) Dot plot showing representative marker gene expression across all 21 cell clusters derived from P7 neonatal rat brain cortex and hippocampus.

(F) Dot plot of representative marker gene expression in neuronal subpopulations.

(G) UMAP visualization of nine neuronal cell populations showing the annotation of each neuronal subtype.

combined for further analysis (Figure S1). Based on a filtering criterion of RNA features >1,000 and mitochondrial gene expression <8.5%, 15,234 nuclei from control and 14,083 nuclei from e-cigarette samples were retained as the final snRNA-seq dataset for all downstream data analyses.

In the snATAC-seq experiment, we captured the chromatin accessibility of 32,000 single nuclei from the P7 brains of eight control (four male and four female pups, 15,834 nuclei) and eight prenatally e-cigarette exposed rat pups (four males and four females, 14,388 nuclei) from four separate snATAC-seq libraries. An average sequence depth of ~71,000 reads and 18,063 fragments were generated per nucleus (Table S1). A custom single-cell ATAC-seq indexed Rn6.0 reference genome (details in Methods) and Cell Ranger ATAC package (version 1.1) were used for mapping and peak calling. In summary, over 65% percent of all reads were confidently mapped to the Rn6.0 genome and over 14% overlapped with their respective transcription start sites (TSS) (Figure S2A and Table S1). The R package Signac (v.1.0.0) was used for cell clustering and differential peak analysis. After applying filtering for ATAC features >1,000, TSS enrichment score >2, and nucleosome signal <1.0% (Figures S2B and S2C), we retained 13,279 nuclei from control and 12,622 nuclei from the prenatally e-cigarette exposed groups, respectively, and merged the data for clustering and downstream analysis. The data retained had a median TSS enrichment score >8, suggesting high quality capture in chromatin regulatory regions (Figure S2C). Of those reads that passed the filtering and mapped to genic regions, over 55% percent were annotated to promoters, 12–13% were annotated to exons and introns, and about 30% were in intergenic regions (Figure S2D). Data from control and prenatally e-cigarette treated groups showed similar sequencing and mapping quality, indicating that minimal bias was introduced between groups during data collection.

Identification of cell types in the developing rat brain

Though many single cell transcriptomic studies have been done on mouse and human brain (Lake et al., 2016; Rosenberg et al., 2018; Fan et al., 2020), little has been done to profile the rat central nervous system (CNS) at the single-cell level. Rats are a widely-accepted animal model for behavioral studies because of their advanced cognition and memory (Iannaccone and Jacob, 2009). Because of the expression differences between rat and mouse genes and the fact that many mouse cell type marker genes are not well annotated in rats, brain cell markers derived from mice might not be useful to identify rat brain cells. This has been a major drawback for researchers who use the rat model for studies of chemical addiction and neurodegenerative diseases, e.g., Parkinson's and Alzheimer's disease. Therefore, better understanding of rat brain at single-cell resolution is needed. To fill this research gap, we characterized the transcriptomic profiles of 29,317 nuclei from control and prenatally e-cigarette exposed rat brains. Using Uniform Manifold Approximation and Projection (UMAP) for dimension reduction and unbiased graph-based clustering, we projected those nuclei into 21 different cell clusters (Figure 1B). We examined the expression of many potential cell type markers extensively and identified each cell type from their distinct expression profiles. Specifically, six clusters showed high-level expression of the excitatory neuron marker *Arpp21* (Luo et al., 2017) (Figure 1C), and three clusters showed high-level expression of known inhibitory neuron markers *Erbb4* and *Gad2* (Luo et al., 2017) (Figure 1D); consequently they were identified as excitatory neuron subtype I-VI and inhibitory neuron subtype I-III, respectively (Figure 1B). We further annotated the remaining clusters based on the expression patterns of well-established cell-specific markers (Ximerakis et al., 2019b; Polioudakis et al., 2019): 3 astrocyte subtype (markers: *Aqp4* and *Slc1a2*), neuroblasts (marker: *Dlx1*), Cajal-Retzius cells (CRs) (markers: *Reln* and *Tp73*), oligodendrocyte progenitor cells (OPCs) (marker: *Cspg4*), microglia (markers: *C1qb*, *Cx3cr1, Iba1*, and *Trem2*), ependymal cells (EPSCs) (markers: *Dynlrb2* and *Dnah12*), perivascular stromal cells (PSCs) (marker: *Col1a1*), neural progenitor cells (NPCs) (markers: *Nusap1* and *Top2a*), and endothelial cells (ECs) (markers: *Cldn5* and *Flt1*) (Figures 1B and 1E). It is worth noting that one cluster did not exhibit a characteristic gene expression pattern other than weak expression for some excitatory and inhibitory neuron marker genes (Figure 1E). Considering the immaturity of the P7 rat brain, we annotated this cluster as immature neurons. The transitional state of those immature neurons was also suggested by their projected proximity to neuron progenitor cells (Figure 1B).

The cerebral cortex is made up of six-layers, from the outermost layer I to the innermost layer VI. The neurons from different cortex layers are formed under strict regulation during embryonic development; these layers exhibit different gene expression profiles (Lake et al., 2016). On the other hand, inhibitory interneurons arise from different regions of the ventral telencephalon, designated as medial, lateral, and caudal ganglionic eminences (MGE, LGE, and CGE, respectively), which display distinctive transcriptomic profiles. To understand these neuronal subtypes better, we examined the gene expression profiles of the six excitatory and three inhibitory neuron clusters and their association with cortical layer position and developmental origin (Figure 1F). Based on the well-known cortical layer (Lake et al., 2016; Luo et al., 2017) and inhibitory interneuron markers (Lake et al., 2016; Polioudakis et al., 2019) (Figures 1F and S3), we annotated the six excitatory neuron subtypes as exL2/3 (excitatory neuron layer 2/3, *Cux1*), exL4 (excitatory neuron layer 4, *Necab1*), exL5 (excitatory neuron layer 5, *Bcl11b* and *Deptor*), exL6 (excitatory neuron layer 6, *Tle4,* and *Foxp2*), exHPN1, and exHPN2 (excitatory neuron hippocampal pyramidal neuron 1 and 2, *Ndst4, Nr3c2,* and *Zbtb20*) (Figures 1G and S3). The three inhibitory neuron clusters were annotated as inCGE (inhibitory CGE-derived interneuron, *Adarb2*), inMGE (inhibitory MGE-derived interneuron, *Sox6* and *Kcnc2*), and inLGE (inhibitory LGE-derived interneuron, *Gnal* and *Dach1*). Of note, after dimension reduction using UMAP, the six excitatory neuron clusters were adjacent to each other; similarly, the three inhibitory neuron clusters were also projected in close proximity (Figure 1G). In addition, the two clusters of hippocampal pyramidal neurons (exHPN1 and exHPN2) were adjacent, whereas the other four clusters of cortical layer projection neurons were contiguous, suggesting diversity of neurons and their interconnection at the transcriptomic level. Overall, the neural and non-neural cell types we uncovered here are highly concordant with previous studies of cell diversity in the cortex and hippocampus (Avey et al., 2018; Artegiani et al., 2017; Zhu et al., 2019). These single-cell transcriptomic data describing the developing rat brain will be an invaluable resource and greatly facilitate future studies of the CNS in the rat, e.g., drug response and neurodegenerative diseases.

Differential gene expression in neonatal neurons after prenatal e-cigarette exposure

All the cell types identified were present with similar cell numbers and proportions in both control and prenatal e-cigarette exposed neonatal brains (Table S2). In addition, the quality of data generated from the

two groups was comparable, with similar numbers of total counts and genes detected per cell (Figures S1–S4 and Table S1). After annotating all the cell types in the snRNA-seq dataset, we investigated the transcriptional changes within the same cell type by performing differential gene expression analysis between the control and e-cigarette groups. Out of ~5,000 total genes detected from all the cell types, 295 unique genes were affected significantly by prenatal e-cigarette exposure in at least one brain cell type [fold change (FC) > 1.2, false-discovery rate (FDR) < 0.2] (Tables S2 and S3). Gene ontology (GO) enrichment revealed that the majority of the 295 differentially expressed genes (DEGs) participated in nervous system development and neuron differentiation, whereas the major cellular component involved was the synapse. Several significant Kyoto Encyclopedia of Genes and Genomes (KEGG) pathways were identified, such as axon guidance, dopaminergic synapse, and glutamatergic synapse (Figure S5), hinting that prenatal e-cigarette exposure imposed profound effects on central nervous system development involving neuronal differentiation and synaptic communication.

Since prenatal e-cigarette exposure exerted only a mild influence on the neuronal transcriptome, we grouped all the nine neuron clusters as excitatory neurons and inhibitory neurons, respectively. We then performed differential expression analysis between prenatal e-cigarette exposed and control nuclei using the combined neuron clusters to increase the statistical power and the number of DEGs. In this manner, we detected 362 DEGs in excitatory neurons and 198 DEGs in inhibitory neurons with a more stringent FDR (<0.1) (Table S5). It is worth noting that calmodulin-binding transcription activator, *Camta1*, was significantly up-regulated in both excitatory and inhibitory neurons after prenatal e-cigarette exposure (FDR = 5.71E-133 and FC = 1.20 in excitatory neurons; FDR = 4.99E-53 and FC = 1.18 in inhibitory neurons, respectively. Figures 2A–2C and Table S5). *Camta1* is known to play a critical role in regulating calmodulin expression and, in turn, maintaining calcium homeostasis (Vuong-Brender et al., 2020). In fact, *Camta1* was significantly elevated in all nine neuron subtypes (Figures 2B, 3D and S6). The expression of another calcium-related gene, the calcium-activated neutral proteinase 13 (*Capn13*), was also increased in inhibitory neurons (FDR = 2.37E-32, FC = 1.17, Figures 2C–2D and Table S5). GO enrichment analyses revealed that the 362 DEGs were enriched in the molecular function of ion or protein binding and were involved in neuron differentiation and axon guidance (Figure 2E). Together, our results suggest that prenatal e-cigarette exposure may adversely affect early CNS development by altering calcium homeostasis and/or calcium signaling pathways.

Prenatal e-cigarette exposure reduced the number of microglia and resulted in glutamate-dependent excitotoxicity

Microglia play a pivotal role in modulating CNS development and maintaining brain (Lenz and Nelson, 2018) function. As the resident immune cells in brain, microglia respond quickly to injury, pathogens, or drugs in a process termed "activation", which results in biochemical and morphological changes away from the homeostatic state. Based on the differential expression analysis, we noticed that more than one-third of all DEGs in the brain induced by prenatal e-cigarette exposure were found in microglia (132 out of total 295 genes) (Table S3). The unusually high number of DEGs observed in microglia was not the result of compromised statistical stringency due to small sample size, since microglia account for about 4.79% of the cell population in our snRNA-seq dataset and its sample size is about the average of all the cell types compared during DEG analysis (4.76% $\pm$ 2.9, Table S2). We speculated that microglia comprised one of the major cell types affected profoundly by prenatal e-cigarette exposure. Therefore, we first examined its population change. We found it striking that prenatal e-cigarette exposure reduced microglial cell number by ~ 22.6%, without changing the cluster projection (Figure 3A and Table S2). To verify this effect, we examined the putative microglia population change in bulk RNA-seq data (collected in a separate but repeated experiment), by using the expression of microglia-specific markers *Trem2* and *Cx3cr1* as indicators of cell population (cell number). The rationale was that the expressions of *Trem2* and *Cx3cr1* are specific to microglia (Figures 1E, 3B, and 3C), and their expression levels per cell are independent of e-cigarette simulation as shown in Figure 3D. Therefore, these markers can be used to reflect the microglia population. In line with the reduction of microglia observed in the snRNA-seq dataset, the expression of *Trem2* and *Cx3cr1* was reduced by 18 and 10%, respectively, at bulk gene expression level after prenatal e-cigarette exposure, with marginal statistical significance ($p = 0.0586$ for *Trem2*, $p = 0.0558$ for *Cx3cr1*) (Figure 3E). This further supports the notion that prenatal e-cigarette exposure reduces the microglia population in early CNS development. We examined the level of another microglial protein, IBA1 (ionized calcium-binding adapter molecule), in P7 whole brain exposed prenatally to e-cigarettes and found it to be significantly down-regulated (Figure 3F) (two-tailed student's t-test, $p = 0.0025$,

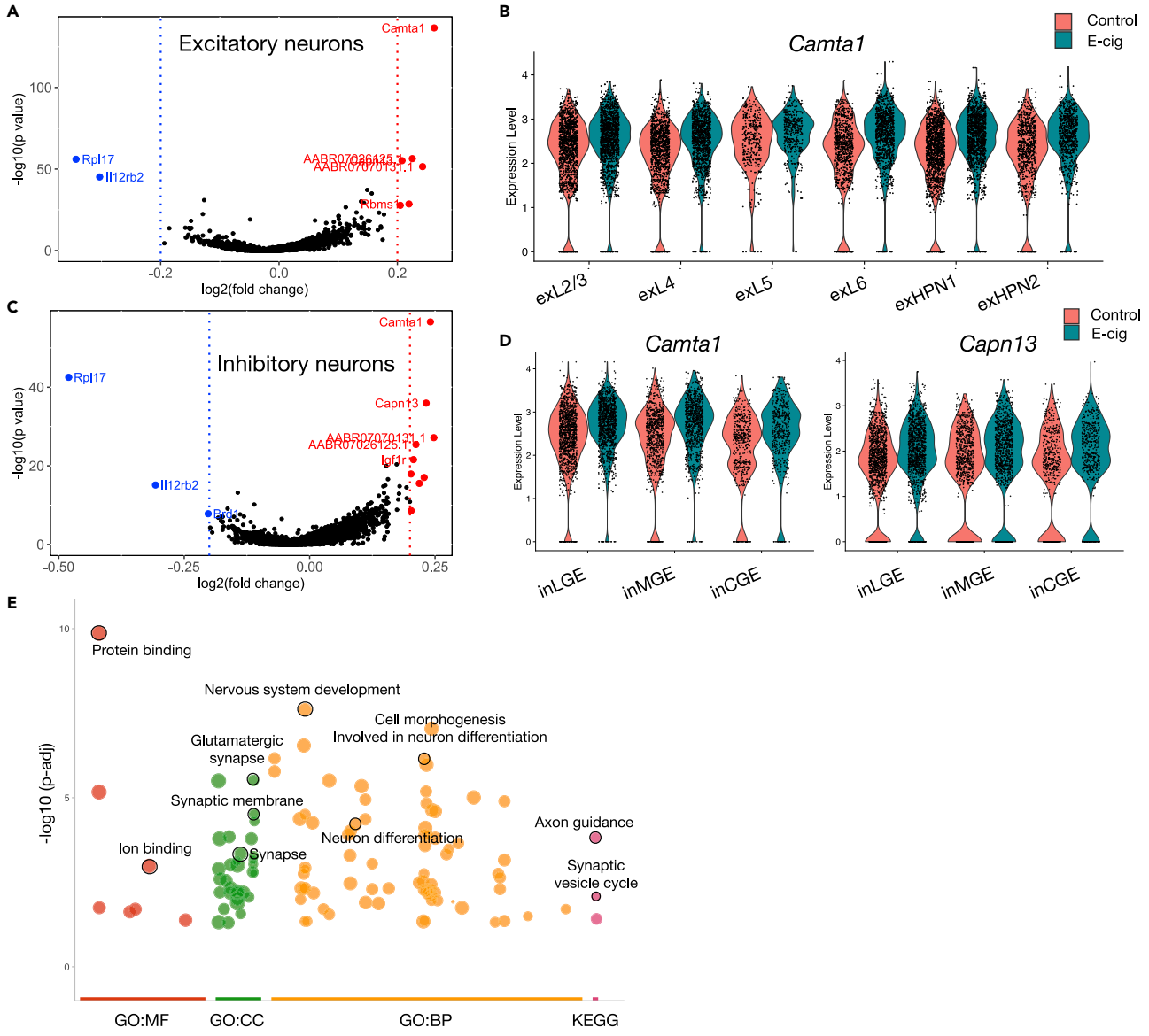

Figure 2. Differential gene expression in excitatory and inhibitory neurons after prenatal e-cigarette exposure

(A and C) Volcano plots showing differentially expressed genes (DE-Gs) in all the excitatory neurons (A) or inhibitory neurons (C) collected from control or maternal e-cigarette exposed P7 rat brains. Blue and red lines indicate log2FoldChange of ±0.2.

(B) Violin plots showing the expression of *Camta1*in six excitatory neuronal subtypes.

(D) Violin plots showing the expression of *Camta1* and *Capn13* in three inhibitory neuronal subtypes.

(E) Manhattan plot showing the top Gene Ontology (GO) terms (MF, molecular function; CC, cellular component; BP, biological process), and Kyoto Encyclopedia of Genes and Genomes (KEGG), enriched from the DE-Gs identified in all neurons between control and e-cigarette exposed P7 rat brains.

n = 10). We speculate that this reduction was due either to microglial death or inhibited microglial proliferation.

Numerous types of neurotransmitter receptors are expressed on microglia, including glutamatergic receptors, GABAergic receptors, and acetylcholine receptors. These receptors allow microglia to communicate with their adjacent neurons. Notably, among the 132 microglia DEGs induced by prenatal e-cigarette exposure (FDR <0.2 and FC > 1.2) (Figure 3G and Table S2), many were glutamate receptors. For instance, the glutamate metabotropic receptor genes, *Grm3* and *Grm7*, as well as the glutamate ionotropic receptor genes, *Grik2* and *Grid2*, were significantly downregulated after prenatal e-cigarette exposure (Figures 3H

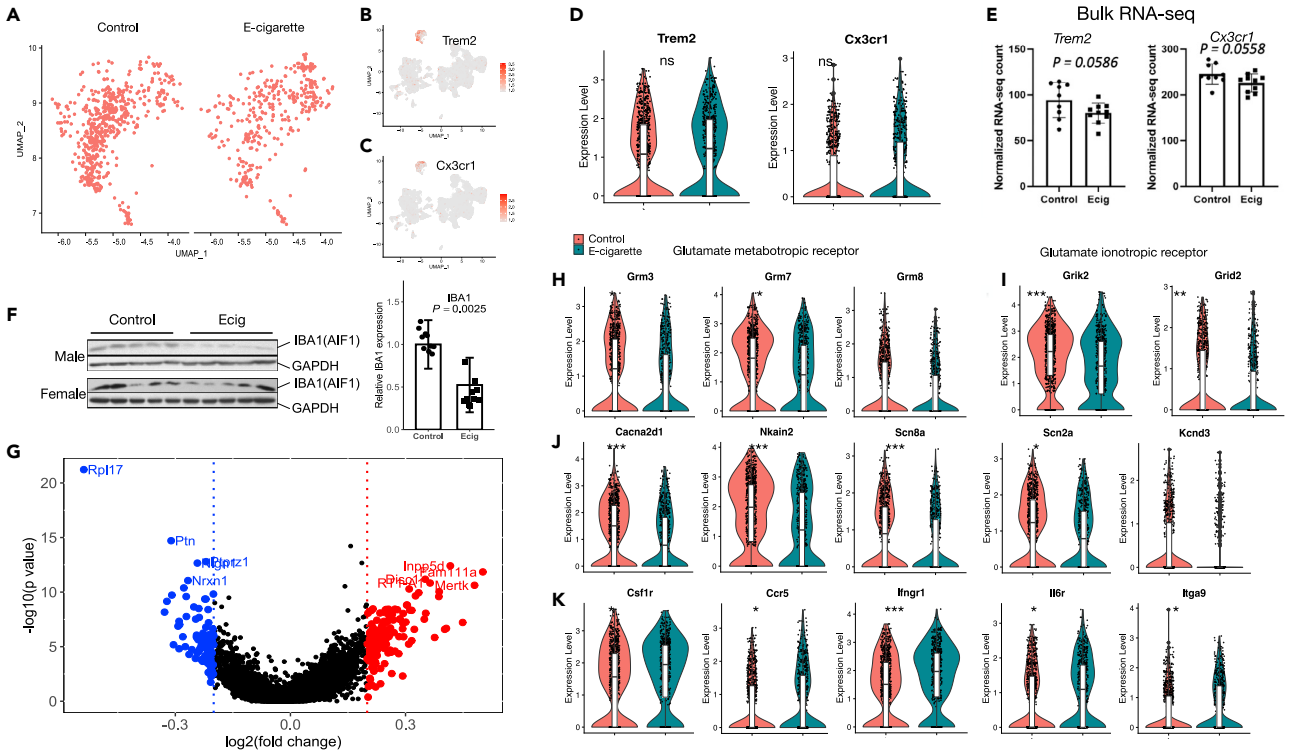

Figure 3. Prenatal e-cigarette exposure reduced the number of microglia and resulted in glutamate-dependent excitotoxicity in the developing brain

(A-C) UMAP plots showing the microglia population in the control and prenatally e-cigarette exposed P7 rat brains, respectively. The specific expressions of microglia markers *Trem2* and *Cx3cr1* are shown in (B) and (C), respectively.

(D) Violin plots with boxplots overlaid showing the expression of *Trem2* and *Cx3cr1* at single-cell level. ns: not significant.

(E) Expressions of *Trem2* and *Cx3cr1* at bulk RNA-seq level shown as normalized RNA-seq counts (trimmed mean of M values normalization, TMM). Control group: n = 9. E-cigarette group: n = 10.

(F) Westernblot of microglia marker IBA1 (also known as AIF1). The relative IBA1 protein level was normalized against internal control protein GAPDH.

(G) Volcano plot showing microglia DE-Gs induced by prenatal e-cigarette exposure. Significantly upregulated genes are highlighted in red and downregulated genes are highlighted in blue. Blue and red lines indicate log2FoldChange of 0.25.

(H–K) Violin plots with boxplots overlaid showing the single-cell level expressions of genes related to (H) glutamate metabotropic receptors, (I) glutamate ionotropic receptors, (J) ion channels, and (K) inflammatory responses from our snRNA-seq dataset. *padj <0.1, **padj <0.01, ***padj <0.001.

Error bars in E and F represent the standard deviations. P values were calculated using two-tailed Student's t-test.

and 3I). In addition, some other ion channel-associated genes, including *Cacna2d1*, *Nkain2*, *Scn8a*, *Scn2a*, and *Kcnd3*, known to contribute to synaptic communication between neurons and microglia, were also markedly downregulated in the microglia of the neonatal brain following prenatal e-cigarette exposure (Figure 3I and Table S3). Meanwhile, the expressions of many chemokines/cytokines and their receptor genes, such as *Ccr5*, *Ifngr1*, *Il6r*, *Itga9*, and *Csf1r*, were increased by 15–24% at cell level in the brains of e-cigarette stimulated rat pups, suggesting elevated neuroinflammation in the developing brain after prenatal e-cigarette exposure (Figure 3K). Overall, our results indicate that prenatal e-cigarette exposure led to glutamate-dependent excitotoxicity followed by inflammatory response in the developing brain. The concerted upregulation of *Csf1r*, an essential indicator for microglial survival, as well as the downregulation of glutamate receptors, might be a homeostatic response, i.e., de-sensitization, of the microglia to prolonged nicotine exposure.

snATAC-seq recapitulates cell identities in the developing rat brain

After QC filtering, a total of 25,901 nuclei from both control and prenatally e-cigarette exposed brains were clustered into 17 different groups based on chromatin accessibility using Latent Semantic Indexing (LSI) (Papadimitriou et al., 2000) dimension reduction techniques (Figure 4A). As there is no chromatin accessibility reference available for the rat to identify brain cells, we relied on the Signac function FindTransferAnchors to generate a set of anchors between our snRNA-seq data (reference) and the

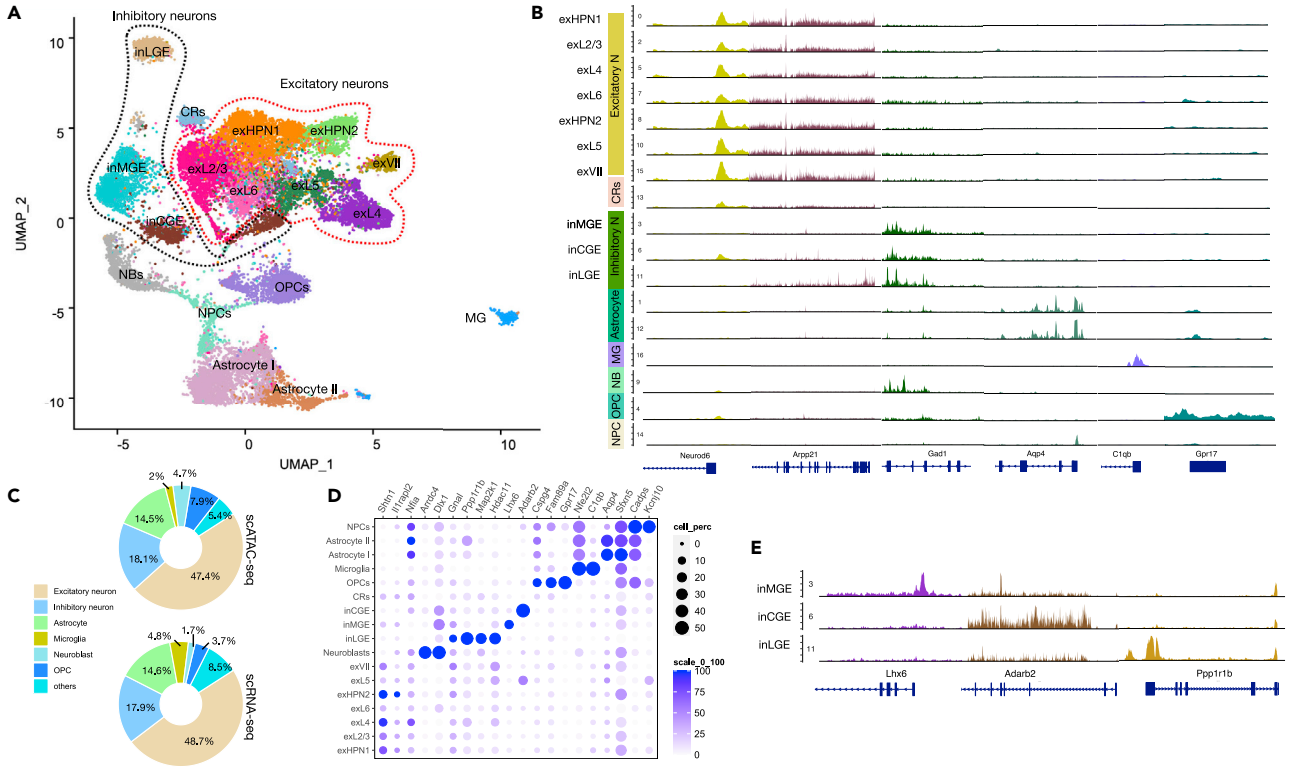

Figure 4. snATAC-seq recapitulates cell identities in the developing rat brain

(A) UMAP showing clusters based on the snATAC-seq dataset of 25,901 nuclei derived from control and prenatally e-cigarette exposed P7 rat brains. Cell type identifications were determined based on snRNA-seq data using cell markers as described in Methods, which were then transferred onto the snATAC clusters using the FindTransferAnchorsfunction in the Signac package. exVII cells were identified manually as there were no counterparts in the snRNA-seq dataset.

(B) Genomic regions showing the snATAC-seq tracks of aggregate chromatin accessibility of representative markers in the major cell types.

(C) Donut plot showing the percentage of major cell types in the snATAC-seq and snRNA-seq datasets.

(D) Dot plot showing the promoter accessibility of representative markers across all 17 clusters in the snATAC-seq data. The accessibility of each gene (column) was scaled from 0 to 100.

(E) Representative genomic regions showing snATAC-seq tracks of aggregate chromatin accessibility across three inhibitory neuronal subtypes.

snATAC-seq data (query), then used TransferData to transfer the cluster identifications onto snATAC-seq clusters. After identification transfer, most of the snATAC-seq clusters were annotated successfully, including six excitatory neuron clusters, three inhibitory neuron clusters, two astrocyte clusters, microglia (MG), neuroblasts (NBs), oligodendrocyte progenitor cells (OPCs), neural progenitor cells (NPCs), Cajal-Retzius cells (CRs), and an unknown cluster (Figure 4A). For the unknown cluster, we tentatively annotated it as exVII based on its similarity with other excitatory neuron types (Figure 4A), and by comparing its chromatin accessibility data with the neighboring clusters and the neuron marker expressions predicted by the Signac GeneActivity function from chromatin accessibility data.

To validate the cell type assignment in our snATAC-seq dataset, we examined the accessibility of selected marker genes from our snRNA-seq data. In line with the prediction, all six excitatory neuron clusters as well as the exVII cluster showed high accessibility at excitatory neuron marker genes *Neurod6* and *Arpp21* (Figure 4B), confirming their excitatory neuron identities. The three inhibitory neuron clusters showed distinctive accessibility at inhibitory neuron marker gene *Gad1* whereas the two astrocyte clusters showed the highest accessibility at the *Aqp4* promoter region. As expected, the *C1qb* promoter region was highly accessible in the microglia cluster, while the OPC marker gene *Cspg4* showed the highest accessibility in OPC cells (Figure 4B). These data not only confirmed the cell identifications in our snATAC-seq dataset, but also demonstrated high concordance between the snRNA-seq and snATAC-seq data. We further compared the major cell type composition in the snATAC-seq data with that in the snRNA-seq data. The snATAC-seq analysis assigned 47.4% of the cells as excitatory neurons, 18.1% as inhibitory neurons, 14.5% as astrocytes, 2% as

microglia, 4.7% as neuroblasts, and 13.3% as OPCs and other cells (Figure 4C). On the other hand, in our snRNA-seq dataset, 48.7% were assigned as excitatory neurons, ~ 17.9% as inhibitory neurons, and ~14.6% as astrocytes. The cellular composition in the snATAC-seq dataset was highly concordant with that in the snRNA-seq dataset (Figure 4C), which further validated our snATAC-seq cell type assignment, and provided support for subsequent downstream analysis, such as trajectory identification.

To establish a set of chromatin accessibility reference markers for neonatal rat brain cell identification, we compared the accessibility of many candidate genes in each cluster extensively and proposed a set of markers with reasonable specificity (Figure 4D). In doing so, we first calculated the means of the normalized promoter accessibilities of the candidate genes in all cells within each cluster, then scaled the data from zero (least accessible) to 100 (most accessible) to enhance the visualization. In general, more specific markers were apparent in glial cells; examples include *Aqp4* and *Sfxn5* for astrocytes, *Nfe2l2* and *C1qb* for microglia, and *Fam89a* and *Gpr17* for OPCs, etc. The markers were less specific and distinctive in neurons due to their closely similar lineages as well as the fact that many neurons were in transition stages in P7 brains. Nevertheless, we were able to identify a few specific chromatin accessibility markers for inhibitory neurons, which included *Lhx6* for MGE-derived inhibitory neurons, *Adarb2* for CGE-derived inhibitory neurons, and *Ppp1r1b* for LGE-derived inhibitory neurons (Figurs 4D and 4E). In addition, we also identified *Arrdc4* and *Dlx1*as unique markers for neuroblasts and *Kcnj10* for neuron progenitor cells (Figure 4D). For certain marker genes that were observed in our snRNA-seq data, such as the pan-inhibitory neuron marker *Erbb4* and the excitatory neuron subtype marker genes *Cux1*, *Il1rapl2*, *Tle4*, *Zbtb20*, and *Tox*, we did not observe noticeable chromatin accessibility changes in the corresponding clusters. Possible explanations were that the gene expression did not always mirror its chromatin accessibility and the turnover of mRNA is likely regulated independently after transcription in different neuron subtypes. In summary, we proposed and presented a set of cell-type specific genes that can be used as chromatin accessibility markers to identify rat brain cells in this study. By combining chromatin markers with expression markers, we propose a convenient yet powerful tool that can be used to profile rat brain cells.

Prenatal e-cigarette exposure promoted neonatal excitatory neural differentiation

After identifying cell types in both snRNA-seq and snATAC-seq datasets with high confidence, we were able to investigate the influence of prenatal e-cigarette exposure on CNS development in a cell type-specific manner. We first investigated the abundance of each cell type and the cellular composition changes between the control and prenatal e-cigarette group using snATAC-seq data, as chromatin accessibility has been demonstrated to be more cell type specific in some instances and thus could capture cell identity better than mRNA expression (Corces et al., 2016; Zamanighomi et al., 2018). In doing so, we calculated the proportion of each major cell type in the control and prenatal e-cigarette groups, respectively (Figure 5A). We found that the microglia in the neonatal brain were reduced by ~40% after prenatal e-cigarette exposure (control: 2.4 $\pm$ 0.03%, e-cigarette exposure: 1.5 $\pm$ 0.05%, $p = 0.005$, Figure 5A). Astrocytes, another major non-neuron cell type, were also reduced significantly after prenatal e-cigarette exposure (control: 15.9 $\pm$ 0.7%, e-cigarette exposure:13.1 $\pm$ 0.4%, $p = 0.027$, Figure 5A). Meanwhile, excitatory neurons and neuroblast cells showed interesting population shifts, with a ~20% increase of excitatory neurons and ~50% reduction of neuroblast cells (Figure 5A). At the neuron subtype level, the fractions of excitatory neurons L2/3 and CGE-derived inhibitory neurons were significantly increased ($p < 0.05$, Figure 5B), whereas the LGE-derived inhibitory neurons were significantly decreased (control: 6.97 $\pm$ 1.98%; e-cigarette exposure:1.09 $\pm$ 2.25%, $p = 0.014$, Figure 5B) after prenatal e-cigarette exposure. For the other neuronal subtypes, except for the excitatory neuron L6, prenatal e-cigarette exposure seemed to increase their population (Figure 5B). Our results unequivocally revealed an extensive effect of prenatal e-cigarette exposure on both neuronal and non-neuronal cells in early CNS development.

To investigate how prenatal e-cigarette exposure affected chromatin accessibility in neonatal brain cells, we performed differential accessibility analysis for each cell type between the control and e-cigarette groups. In neonatal brains, prenatal e-cigarette exposure resulted in the greatest chromatin accessibility changes in the excitatory neurons, with 978 differentially accessible regions (DARs) (FC > 1.2 and $p < 0.001$) detected; the vast majority were prone to more openness (Figure 5C). Similar patterns were observed in inhibitory neurons, astrocytes, OPCs, and neuron progenitor cells. Chromatin accessibility analysis suggested that prenatal e-cigarette exposure had long-lasting, broad effects on CNS transcription in many types of cells, particularly on promoting transcription, e.g., e-cigarette exposure promoted more chromatin opening than closing. This was in line with our snRNA-seq results, which showed that the

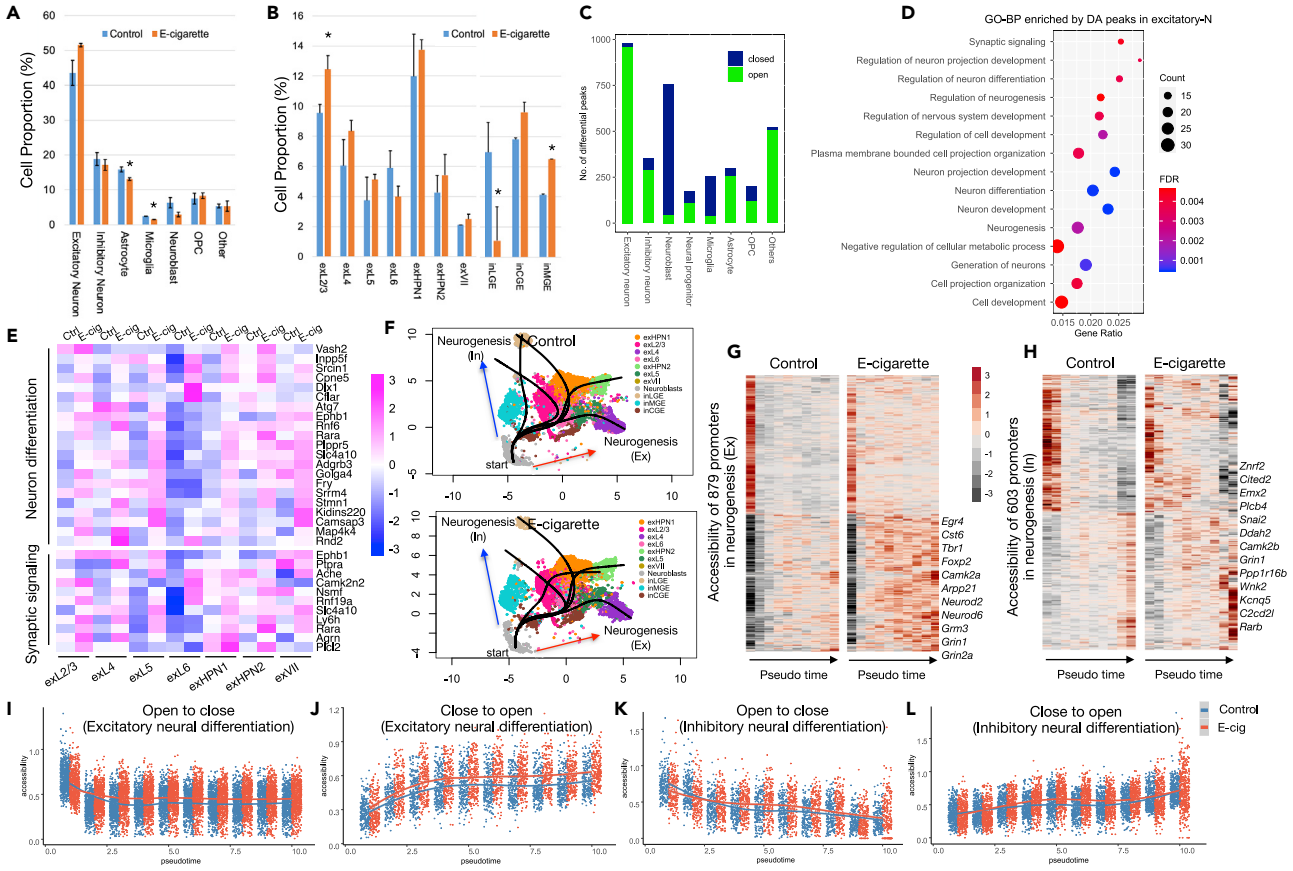

Figure 5. Prenatal e-cigarette exposure promoted neonatal neuronal differentiation

(A and B) Bar plot showing the cell composition of (A) *major* cell types and (B) neuronal subtypes in both control and prenatal e-cigarette exposed P7 rat brains. Data were calculated from the snATAC-seq dataset and presented as mean ± SD (*p < 0.05 by one-tailed t-test).

(C) Number of differential accessible chromatin regions (DARs) in the major cell types. Blue: chromatin regions with significantly reduced accessibilities after prenatal e-cigarette exposure; green: chromatin regions with significantly increased accessibilities after prenatal e-cigarette exposure.

(D) Dot plot showing the top Gene Ontology (GO) biological process (BP) terms enriched from genes with DARs in excitatory neurons.

(E) Heatmap of promoter accessibility of genes enriched in neuron differentiation and synaptic signaling processes in six excitatory neuron subtypes. The relative chromatin accessibility at promoter regions were row scaled and clustered by the "median" method.

(F-H) Trajectory of neuron differentiation in control (top) and prenatal e-cigarette exposed (bottom) samples. The dynamic changes of promoter accessibility of genes involved in (G) excitatory and (H) inhibitory neuronal differentiation according to pseudotime. Cells on each differentiation trajectory were divided into ten quantiles according to their trajectory pseudotime as calculated from Slingshot. DARs were determined from cells between the starting point (neuroblasts) and the endpoints (exL4 and exVII for excitatory neurons, and inLGE for inhibitory neurons). The assignment of DARs to their promoters was visualized by a row scaled heatmap.

(I–L) Scatterplots showing the trend of promoter accessibility change over neuronal differentiation. The DARs were determined as described in G and H, and those annotated to gene promoters are shown on plots. Locally weighted smoothing (LOESS) was used to reveal the trend in the accessibility over pseudotime.

expressions of many genes were elevated in those types of cells (Table S3). Interestingly, prenatal e-cigarette exposure seemed to have the opposite effect on chromatin accessibility in microglia and neuroblasts compared with other types of cells, i.e., e-cigarette exposure induced more chromatin closing. Chromatin closing (216 closed vs. 45 open) in microglia supports the view that nicotine inhibits microglia activation and brain inflammation (Noda and Kobayashi, 2017). Prenatal e-cigarette exposure induced promoter closing at a significant number of genes in neuroblasts (710 closed vs. 45 open) suggesting a strong effect on neuron differentiation, which might lead to the cell population changes observed earlier.

Next, we focused on the differences in chromatin accessibility in excitatory neurons since they are the most abundant cell type in the brain and had the most DARs induced by prenatal e-cigarette exposure. To understand the biological significance of those DARs, we first annotated the DARs to rn6.0 genes using the

R package 'annotatr' (v1.10.0), then conducted gene ontology (GO) analysis on those genes. In agreement with the snRNA-seq data, GO enrichment of DAR linked genes showed that neuron differentiation, synaptic signaling, and neuron projection development were the biological processes most influenced by e-cigarette exposure in the excitatory neurons (Figure 5D). This agreed well with functions enriched by DEGs (Figure 2E) and further corroborated our findings from the snRNA-seq data. In fact, enhanced chromatin accessibility for the genes involved in neuron differentiation and synaptic signaling was observed in all excitatory neuron subtypes in the prenatal e-cigarette exposure group; these genes were consequently very likely to promote excitatory neuron differentiation. A few examples of such genes include *Camsap3*, *Stmn1*, *Dlx1*, *Camk2n2*, *Ly6h*, etc. (Figure 5E). Two examples were the promoter region of *Camsap3* (calmodulin-regulated spectrin-associated protein 3), which plays a key role in maintaining neuronal polarity and was significantly more accessible in the exL2/3 cluster, and the promoter accessibility of *Camk2n2*, another calmodulin-dependent gene, which was significantly increased in the exL6 cluster after prenatal e-cigarette exposure. *Camk2n2* not only regulates neuronal synaptic plasticity, but also may act to inhibit the phosphorylation of AMPA receptors. These data suggest strongly that prenatal e-cigarette exposure may accelerate neuronal differentiation and maturation in the neonatal brain.

To study the influence of e-cigarette exposure on neuronal differentiation dynamics and lineage progressions, we applied the Slingshot algorithm (Street et al., 2018) to infer cellular trajectory and pseudotime from our snATAC-seq data. All ten neuronal subtypes and neuroblasts were included for the analysis. In brief, the number of cell lineages, bifurcation points, and the pseudotime of each cell on the lineage trajectory were calculated with the Slingshot function using neuroblasts as the starting point. Multiple lineages from neuroblasts to potential endpoints were predicted. Despite the similarity of the predicted trajectories in control and exposure groups, the cellular trajectories bifurcated into excitatory or inhibitory destinations earlier in the control group (Figure 5F), and those trajectories were more widely separated in excitatory neurons, i.e., the more differentiated state. On the other hand, the inhibitory neuron trajectory was shifted to an excitatory neurogenesis destination in the exposure group (Figure 5F). These data suggested that prenatal e-cigarette exposure might promote excitatory neuron differentiation or hinder inhibitory neuron differentiation, which was consistent with the larger proportion of excitatory neurons observed in the prenatal e-cigarette exposed neonatal brain (Figure 5A).

Knowing that prenatal e-cigarette exposure influences neuronal differentiation, we next examined the temporal dynamics of chromatin accessibility for neuronal differentiation genes. First, we identified all genes with differential promoter accessibility in the excitatory neuron trajectory (start point: neuroblasts, endpoint: exVII, 807 genes, Figure 5G) and the inhibitory neuron trajectory (start point: neuroblasts, endpoint: inLGE, 603 genes, Figure 5H). Second, we grouped the neurons into 10 quantiles based on their pseudotime as calculated from trajectory prediction. Finally, we calculated the average promoter accessibility for each gene from all cells within a given quantile and visualized the accessibility changes according to their pseudotime. We found that during both excitatory and inhibitory neuron differentiation, there was a rapid chromatin closing (accessibility of promoters from open to closed, Figure 5I), as well as slower opening of certain chromatin regions (accessibility of promoters from closed to open, Figure 5J). For excitatory neuron differentiation, the opening of the promoters' accessibility occurred earlier in the e-cigarette cells, and the openness was greater compared with control cells (Figures 5G–5J). For example, *Neurod2*, known to play a role in neuronal differentiation and which is expressed in mature neurons (Preissl et al., 2018), showed increased accessibility in cells from the e-cigarette group. Other mature neuron specific genes, including *Neurod6*, *Arpp21*, and certain glutamate receptor related genes such as *Grin1*, *Grin2a*, *Grm3*, showed greater accessibility at promoter regions in the e-cigarette group. In contrast, we did not observe much difference in the dynamic process of chromatin closing between control and e-cigarette groups in inhibitory neurons (Figure 5H). During the inhibitory neuron differentiation, promoters opened at similar stages in control and e-cigarette groups, although greater openness was seen in cells from the prenatal e-cigarette exposure group (Figure 5L). Of note, chromatin closing during inhibitory neuron differentiation was delayed in the e-cigarette group (Figure 5K) at certain promoter regions, such as *Hat1* and *Cited2*; this may be related to delayed differentiation in affected subpopulations. Altogether, our study showed that prenatal e-cigarette exposure promotes neonatal excitatory neuron differentiation while slowing the generation of LGE-derived inhibitory neurons.

Prenatal e-cigarette exposure induced microglial cell death and elevated susceptibility to cerebral ischemic injury

Reduction of the microglia population by prenatal e-cigarette exposure was observed in both our snRNA-seq data and snATAC-seq data. However, the underlying mechanism is not known. Previous studies

indicated that nicotine inhibits microglial proliferation (Guan et al., 2015). To understand how e-cigarette exposure affected the microglia population, we used our snRNA-seq data to analyze the cell cycle in microglia. In brief, each microglial cell was assigned to a cell cycle state based on the expression of cell cycle transcripts using Seurat function CellCycleScoring and the list of cell cycle markers proposed by Tirosh (Tirosh et al., 2016). We then applied Fisher's exact test to the number of microglia at each cell cycle between the control and e-cigarette groups to determine whether prenatal e-cigarettes affected microglial proliferation in the developing brain. We found that there was no statistically significant difference in the microglial cell cycle stages between the control and e-cigarette groups ($p = 0.835$ for G1; $p = 0.616$ for G2M; $p = 0.937$ for S, Figure S7). Microglial cells in the P7 rat brains were predominantly in G1, ~50% in control and ~52.8% in the e-cigarette group. Microglia in S were slightly reduced in the prenatal e-cigarette exposed brain, but the difference was not statistically significant (control versus e-cigarette: 28.9 vs. 25.9%, Figure S7). Next, to determine the biological functions associated with the chromatin accessibility changes induced by prenatal e-cigarette exposure in microglia, we annotated the DARs in microglia followed by gene ontology (GO) analysis. Interestingly, response to stress (GO:0033554 and GO:0006950) and cellular response to DNA damage stimulus (GO:0006974) were enriched in microglia (Figure 6A). Ingenuity Pathway Analysis (IPA) further revealed reduced synaptogenesis signaling and glutamate receptor signaling, as well as increased NFAT regulated immune response (Figure 6B).

We also examined transcription factor binding motifs from DNA sequences in DARs induced in neurons and microglia due to prenatal e-cigarette exposure. We identified all six transcription factor binding motifs (*jaspar 2020* database) in neurons and microglia from the DARs induced by prenatal e-cigarette exposure (Table S6). Biological functions of those motif binding transcription factors all correlated well with e-cigarette induced changes. For instance, *Nfatc2* (nuclear factor 2 of activated T cells), which plays a central role in inducing gene transcription during the immune response, is dependent on calcium-dependent activation of calcineurin signaling. *Nfatcs* is involved in numerous cellular functions such as apoptosis and the cell cycle (Mognol et al., 2016). This is consistent with the observation of the alteration of cell population and cell communication in microglia in prenatal e-cigarette exposed brains (Figures 5A and 6). Another example is *Nr4a2*, nuclear receptor subfamily 4 group A member 2 (also called Nurr1) (Figure 6C). *Nr4a2* is known to regulate cellular proliferation and apoptosis, as well as help maintain the dopaminergic system in the brain. Mutations in this gene have been associated with disorders related to dopaminergic dysfunction, including Parkinson's disease and schizophrenia (Singh et al., 2020).

Previous studies suggested that microglia protect the CNS against injury. For example, elimination of microglia increased inflammation and superoxide production and exacerbated post-ischemic brain injury (Szalay et al., 2016; Jin et al., 2017; Faustino et al., 2011). To determine whether the reduction of microglia caused by prenatal e-cigarette exposure would enhance the susceptibility of neonates to cerebral ischemic injury, we performed a transient middle cerebral artery occlusion (tMCAO) experiment in the P9 rats that were subject to prenatal e-cigarette exposure. Strikingly, we observed a more than 70% increase in infarct size in the neonatal brains with prenatal e-cigarette exposure compared to the air exposure control ($13.8 \pm 3.9\%$ relative infarct area in the control brains vs. $23.8 \pm 1.9\%$ in brains prenatally exposed to e-cigarette vapor, two-tailed t-test, $p < 0.001$, Figure 6D). Sham controls showed that the surgery itself did not cause cerebral ischemic injury (Figure S8).

DISCUSSION

Here we provided comprehensive single-cell transcriptome and chromatin accessibility analysis of the developing rat brain (combined neocortex and hippocampus regions) with and without prenatal e-cigarette exposure. Numerous studies have established that *in utero* nicotine exposure may impact brain development and consequently result in neuro-developmental abnormalities, including increments in cell density in the hippocampus (Roy et al., 2002) and reduced volumes of cortical gray matter in offspring (El Marroun et al., 2014). Offspring exposed to smoking after birth do not exhibit the same adverse trajectories (Wakschlag et al., 2002), suggesting different biologically mediated mechanisms during gestation. In this study, we provided *in vivo* evidence that prenatal e-cigarette exposure promoted excitatory neuronal differentiation and increased excitatory neuronal cell composition in the developing rat brain. Exploiting single-cell ATAC-seq and single-cell transcriptome analysis, we identified changes in different neuronal subtypes after prenatal e-cigarette exposure in great detail. Specifically, we found that after prenatal e-cigarette exposure, most of the excitatory neuron subtypes as well as MGE- and CGE-derived inhibitory neurons were increased in number, except for LGE-derived inhibitory neurons, which were decreased. In

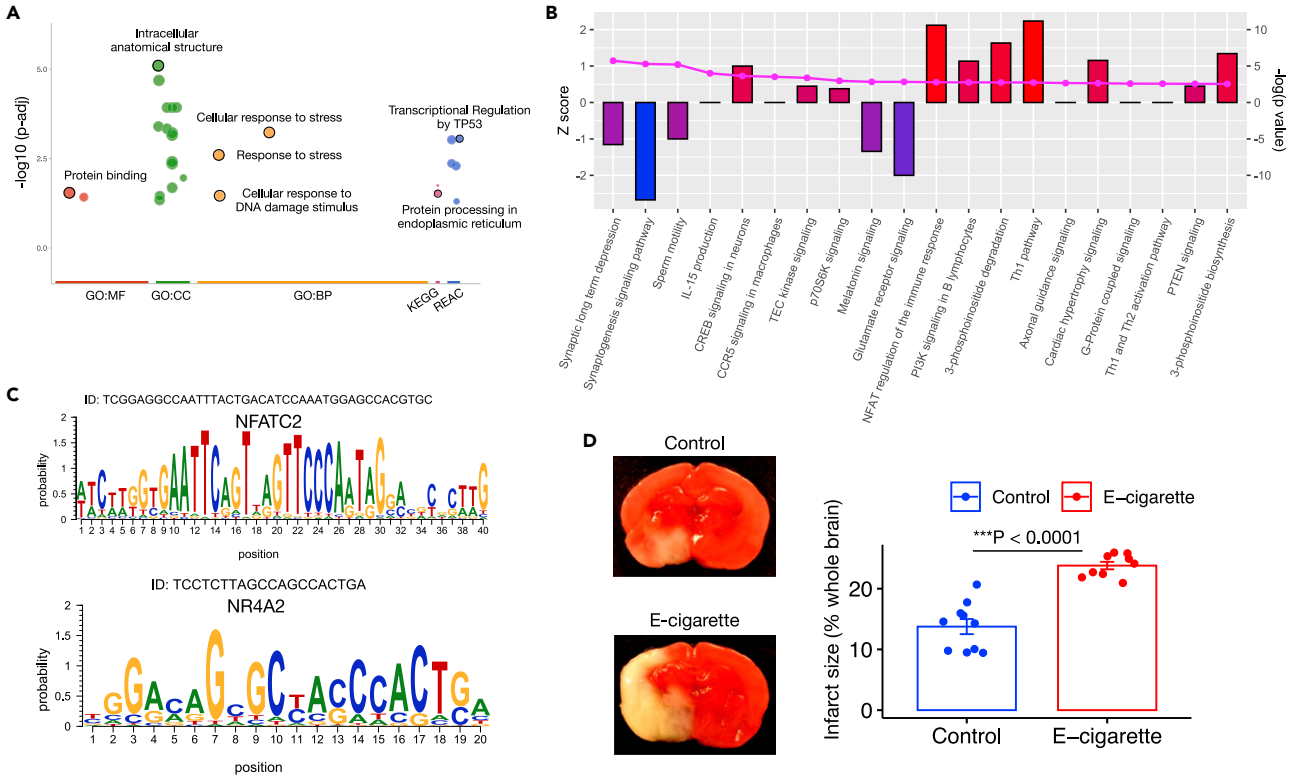

Figure 6. Prenatal e-cigarette exposure induced microglial cell death and elevated susceptibility to cerebral ischemic injury

(A) Manhattan plot showing the top Gene Ontology (GO) terms (MF, molecular function; CC, cellular component; BP, biological process), Kyoto Encyclopedia of Genes and Genomes (KEGG), and Reactome, enriched from the genes within DARs in microglia between control and e-cigarette exposed P7 rat brains.

(B) IPA using DE-Gs determined in microglia (snRNA-seq dataset) between control and e-cigarette exposed P7 rat brains.

(C) Enrichment of the transcription factor binding motifs from microglia differential peaks. The height of the letters was scaled to the frequency of each base at a given position.

(D) Prenatal e-cigarette exposure aggravated neonatal cerebral ischemic injury. Transient Middle Cerebral Artery Occlusion (tMCAO) was conducted on the postnatal day 9 rat pups of both genders with or without prenatal e-cigarette exposure. The brain infarct size was determined by TTC staining 48 h after tMCAO. The Relative infarct areas (calculated as the ratio of infarct area to the total brain area studied) were shown as Means ± SD in the barplot. ***p < 0.001, e-cigarette exposure versus control. Control group: n = 5 male and 5 female pups. E-cigarette group: n = 4 male and 5 female pups. P values were calculated using two-tailed Student's t-test.

search for an explanation, we discovered that the neuronal differentiation lineage trajectory shifted from inLGE towards excitatory neurons in the prenatal e-cigarette exposed offspring (Figure 5F). Consistent with shifting neuronal trajectory, prenatal e-cigarette exposure altered the promoter accessibility of many genes involved in neuronal differentiation over pseudotime. When neuroblasts were used as the neuronal differentiation start point, the opening of chromatin loci at endpoint genes (expressed in differentiated neurons) occurred earlier and faster (Figure 5G) in the cells from the e-cigarette exposure group. While this was true for both excitatory and inhibitory neurons, the change was more pronounced in excitatory neurons (Figure 5H), resulting in stronger influence on neuronal differentiation genes in the excitatory neurons over pseudotime. As nicotine's effect on shifting neuronal proliferation to differentiation was observed both in *in vivo* (Dwyer et al., 2008) and *in vitro* (Lee et al., 2014) studies, we assume that nicotine is the active ingredient in e-cigarette that influences neuronal differentiation in our study. In summary, we found that prenatal e-cigarette exposure affects neuronal differentiation, which may result in loss of LGE-derived inhibitory neurons and excitatory-inhibitory imbalance in certain brain regions.

In addition to promoting excitatory neuron differentiation, our data also indicated that prenatal e-cigarette exposure accelerated maturation of neuronal synaptic function in the immature brain. Early CNS development involves neuronal differentiation and neural circuitry maturation. Many critical developmental events occur during the 22 days of gestation in rats, including early synaptogenesis. In the immature brain,

connectivity between many neurons has not been established. Many immature synapses are "silent" and do not produce AMPA-mediated excitatory postsynaptic potentials (EPSPs). Previous reports suggested that a single exposure to nicotine causes persistent changes in synaptic efficacy in immature glutamatergic synapses (Maggi et al., 2003). In the neonatal rat hippocampus, nicotine-mediated glutamate release can produce EPSPs in immature synapses, which converts 'silent' synapses to functional synapses (McKay et al., 2007). In our study, both snRNA-seq and snATAC-seq data showed that glutamatergic synapses and synaptic signaling were highly enriched in GO analysis. The accessibility of synaptic signaling associated loci such as *Nsmf, Ly6h,* and *Plcl2* were increased after prenatal e-cigarette exposure, suggesting accelerated synaptic maturation.

Calcium is a ubiquitous key signaling element in neurons. It regulates diverse physiological processes in the brain, including cell differentiation, proliferation, apoptosis, excitation, and neuronal plasticity. By integrative analysis of the single-cell transcriptome and chromatin accessibility of neonatal rat brain cells exposed to prenatal e-cigarette vapor, we delineated differential gene expression and the corresponding chromatin accessibility changes in each specific cell type/neuronal subtype. Single-cell level DEG and DAR analysis pointed to differential genes linked to calcium signaling in many cell types, including neuron and microglia (Table S3, S4 and S7).

We proposed that interruption of calcium signaling plays a central role in the adverse biological responses induced by prenatal e-cigarette exposure in early CNS development. This concept is supported by many lines of evidence. First, nicotine, the major addictive substance in e-cigarette vapor, structurally resembles the neurotransmitter acetylcholine and binds to nicotinic acetylcholine receptors (nAChRs). Neuronal nAChRs start to appear early in gestation (Zoli et al., 1995; Adams et al., 2002; Hellstrom-Lindahl et al., 1998) and are abundant in the CNS. Second, stimulation of presynaptic nAChRs by nicotine results in calcium influx through nAChRs or voltage-dependent calcium channels (VDCCs). Influx of calcium modulates synapse signaling and calcium-dependent transcription (Greenberg et al., 1986) through calcium/calmodulin signaling. Third, we found that *Camta1* (Calmodulin-binding transcription activator 1) was the most highly elevated DEG in all nine neuron subtypes in the offspring of the e-cigarette-exposed brains (Figure 2). *Camta1* is regulated by calcium/calmodulin-dependent kinase (CaMK) (Vuong-Brender et al., 2020). We reasoned that the influx of calcium mediated by nAChRs is sensed by calmodulin, which subsequently activates CaMK signaling and promotes *Camta1* expression. Camta1 functions as a transcription activator and co-activator involved in cell growth suppression, neuronal differentiation (Henrich et al., 2011), regulation of calmodulin abundance and control of Ca^{2+} homeostasis, stress response etc. Finally, besides *Camta1*, other calcium/calmodulin dependent genes were also differentially expressed, including *Capn13*, *Camk2a*, *Camk2b*, *Camk2d*, *Camk1*, etc. (Table S3). Some key elements in calmodulin signaling pathways, such as the *Campasp3* and *Camk2n2* genes, were also identified in neurons by independent DAR analysis from snATAC-seq data (Table S4). Because calcium influx into neurons enhances neurotransmitter release (such as dopamine, glutamate, etc.) and activates CREB, this explains the observed enrichment in those processes (Figure S4). In summary, our study strongly supports the view that prenatal e-cigarette exposure causes calcium influx and overload in the developing neurons, alters calcium/calmodulin signaling, and subsequently changes the neuronal differentiation trajectory in neonatal rat brain. Future study is needed to identify the *Camta1* downstream target genes in the developing brain in response to prenatal e-cigarette exposure.

Another important finding in our study was that the microglial population was reduced in the developing brains of offspring after prenatal e-cigarette exposure. Previous studies suggested that nicotine inhibits microglial proliferation *in vitro* in an α7 nAChR-dependent manner (Guan et al., 2015). This suggests the interesting possibility that the reduction of microglia we observed resulted from nicotine inhibition of microglial proliferation through the α7 nAChR. Since we did not find any difference in the expression of *Chrna7* (α7 nAChR encoding gene) at the single-cell level between control and e-cigarette exposure groups, we concluded that prenatal e-cigarette exposure does not inhibit the expression of α7 nAChR. In addition, there was no statistical difference between the microglial cell cycle states in the brains between control and prenatal e-cigarette exposure groups, suggesting that other mechanisms are involved instead of direct inhibition of microglial proliferation. IPA using DEGs from microglia showed that canonical immune pathways were upregulated in microglia after prenatal e-cigarette exposure (Figure 6B), indicating the activation of microglia in response to e-cigarette exposure. In addition, the enrichment analysis from DAR linked genes showed that the responses to stress and DNA damage were the primary biological

responses (Figure 6A). Based on these observations we believed that prenatal e-cigarette exposure activates microglia in the neonatal rat brain, which might lead to DNA damage to microglia, and consequently cell death. This was further supported by the TP53 signaling pathway identified by Reactome (REAC) enrichment analysis (Figure 6A), hinting that the apoptotic pathway was likely activated in microglia after prenatal e-cigarette exposure.

Recent studies have revealed exciting functional diversity of microglia during brain development. In addition to the well-known immunological functions, microglia also guide neural development and help shape neuronal circuits, in part by sensing local changes in the brain microenvironment and by interacting with developing neurons (Schafer and Stevens, 2015). In this study, we found that the expression of many glutamate receptors such as *Grm3, Grm7, Grm8, Grik2*, and *Grid2* was downregulated in microglia after prenatal e-cigarette exposure, which could be due to excessive glutamate released from presynaptic termini in response to nicotine stimulation, possibly associated with impaired microglia-neuron communication. The compromised microglia-neuron interactions may also prevent the microglia from acting against excitotoxic neuronal injury, since microglia are known as endogenous brain defenders after brain injury (Faustino et al., 2011; Jin et al., 2017; Szalay et al., 2016). Depletion of microglia exacerbates inflammatory responses, leukocyte infiltration, and cell death during brain ischemia (Jin et al., 2017). Moreover, microglia are reported to modulate intracellular calcium load in neurons (Cserép et al., 2020), whereas absence of microglia was shown to dysregulate neuronal calcium responses, leading to calcium overload (Szalay et al., 2016). In our study, the reduced microglia population, impaired microglia-neuron interactions, and aberrant calcium signaling following prenatal e-cigarette exposure all could contribute to increased susceptibility to brain injury. This is in line with recent observations reported in a neonatal hypoxia-ischemia mouse model, in which a worse brain injury outcome was observed in the prenatally e-cigarette exposed offspring as a result of reduced brain glucose utilization (Sifat et al., 2020). How e-cigarette vapor affects microglial sensing and regulation of neuronal activity is presently unclear. Whether reduced microglia after prenatal e-cigarette exposure will affect long-term functional synaptic formation and neural circuitry needs to be determined in future studies.

In summary, we used single-cell RNA-seq and ATAC-seq to provide a comprehensive landscape of cellular and molecular alterations of neonatal rat brains that were exposed to e-cigarette vapor *in utero*. We showed that prenatal e-cigarette exposure distorted neuronal lineage differentiation, resulting in an increased excitatory neuronal composition. Furthermore, prenatal e-cigarette exposure disrupted calcium signaling and calcium homeostasis, diminished the number of microglia in the developing brain, and importantly, elevated susceptibility to neonatal cerebral ischemic injury as demonstrated by the tMCAO results in Figure 6D. Due to the different development stage of neocortex and hippocampus, and their possible divergent responses to e-cigarette exposure, future study is needed to delineate the impact on each specific brain region. We believe these findings provide important new insight into the mechanisms responsible for abnormal brain development in offspring of animals exposed to e-cigarette vapor, which will help explore promising molecular and cellular therapeutic targets for treating nicotine-induced brain damage.

Limitations of the study

Due to the heterogeneity and complexity of brain cells, we only included prefrontal cortex and hippocampus in this study. Therefore, the influence of prenatal e-cigarette exposure on brain development, i.e., neuronal development, was limited to these regions. In addition, single nucleus transcriptome analysis detects limited numbers of genes, thus fewer cell markers were available when snRNA-seq was used to profile brain cells.

STAR★METHODS

Detailed methods are provided in the online version of this paper and include the following:

- KEY RESOURCES TABLE
- RESOURCE AVAILABILITY
  - Lead contact
  - Material availability
  - Data and code availability
- EXPERIMENTAL MODEL AND SUBJECT DETAILS
- METHOD DETAILS

- Prenatal e-cigarette exposure
- Brain tissue dissection, single nucleus isolation, and capture
- Library sequencing
- snRNA-seq data analysis
- snATAC-seq data analysis
- snRNA-seq and snATAC-seq integration analysis
- Cell lineage and neuron differentiation in pseudotime
- Custom indexed reference genomes for rat single nucleus RNA-seq and ATAC-seq
- Canonical pathway and molecular function analysis
- Transient middle cerebral artery occlusion (tMCAO)
- Measurement of infarct size
- Western blotting analysis

● QUANTIFICATION AND STATISTICAL ANALYSIS

SUPPLEMENTAL INFORMATION

Supplemental information can be found online at https://doi.org/10.1016/j.isci.2022.104686.

ACKNOWLEDGMENTS

The study was funded in part by the National Institutes of Health (NIH) grants S10OD019960 (CW), HL135623 (DX), HD088039 (DX), the American Heart Association (AHA) grant 18IPA34170301 (CW), the Ardmore Institute of Health grant 2150141 (CW) and Dr. Charles A. Sims' gift to the LLU Center for Genomics. We would also like to thank the partial support of the Loma Linda University School of Medicine GCAT grant (CW).

AUTHOR CONTRIBUTIONS

CW conceived study, and CW and DX designed the experiments. ZC, WC, and YL performed experiments including animal *in vivo* model, single nucleus isolation, library constructions and sequencing. WC and ZC drafted the manuscript and performed bioinformatics data analyses. CW, MMJ, and DX edited and revised the manuscript. ZC and YL prepared the methods for the manuscript. All authors reviewed and approved the manuscript. CW finalized and submitted the manuscript.

DECLARATION OF INTERESTS

All authors claim no conflicts of interest.

Received: January 28, 2022
Revised: May 13, 2022
Accepted: June 24, 2022
Published: August 19, 2022

REFERENCES

Droit, A., Gottardo, R., Robertson, G., and Li, L. (2021). GADEM: de novo motif discovery (Bioconductor).

Adams, C.E., Broide, R.S., Chen, Y., Winzer-Serhan, U.H., Henderson, T.A., Leslie, F.M., and Freedman, R. (2002). Development of the α7 nicotinic cholinergic receptor in rat hippocampal formation. Dev. Brain Res. *139*, 175–187. https://doi.org/10.1016/s0165-3806(02)00547-3.

Alkam, T., Kim, H.-C., Mamiya, T., Yamada, K., Hiramatsu, M., and Nabeshima, T. (2013). Evaluation of cognitive behaviors in young offspring of C57BL/6J mice after gestational nicotine exposure during different time-windows. Psychopharmacology *230*, 451–463. https://doi.org/10.1007/s00213-013-3175-9.

Butler, A., Hoffman, P., Smibert, P., Papalexi, E., and Satija, R. (2018). Integrating single-cell transcriptomic data across different conditions, technologies, and species. Nat. Biotechnol. *36*, 411–420. https://doi.org/10.1038/nbt.4096.

Artegiani, B., Lyubimova, A., Muraro, M., Van Es, J.H., Van Oudenaarden, A., and Clevers, H. (2017). A single-cell RNA sequencing study reveals cellular and molecular dynamics of the hippocampal neurogenic niche. Cell Rep. *21*, 3271–3284. https://doi.org/10.1016/j.celrep.2017.11.050.

Avey, D., Sankararaman, S., Yim, A.K., Barve, R., Milbrandt, J., and Mitra, R.D. (2018). Single-cell RNA-seq uncovers a robust transcriptional response to morphine by glia. Cell Rep. *24*, 3619–3629.e4. https://doi.org/10.1016/j.celrep.2018.08.080.

Baeza-Loya, S., Viswanath, H., Carter, A., Molfese, D.L., Velasquez, K.M., Baldwin, P.R., Thompson-Lake, D.G.Y., Sharp, C., Fowler, J.C., De La Garza, R., and Salas, R. (2014). Perceptions about e-cigarette safety may lead to e-smoking during pregnancy. Bull. Menninger Clin. *78*, 243–252. https://doi.org/10.1521/bumc.2014.78.3.243.

Casserly, A.P., Tsuji, J., Zhao-Shea, R., Smith, C.B., Molas, S., Tapper, A.R., Weng, Z., and Gardner, P.D. (2020). Integrated miRNA-/mRNA-Seq of the habenulo-interpeduncular circuit during acute nicotine withdrawal. Sci. Rep. *10*, 813. https://doi.org/10.1038/s41598-020-57907-w.

Chen, H., Li, G., Chan, Y.L., Chapman, D.G., Sukjamnong, S., Nguyen, T., Annissa, T., Mcgrath, K.C., Sharma, P., and Oliver, B.G. (2018a). Maternal e-cigarette exposure in mice alters DNA methylation and lung cytokine expression in

offspring. Am. J. Respir. Cell Mol. Biol. *58*, 366–377. https://doi.org/10.1165/rcmb.2017-0206rc.

Chen, H., Li, G., Chan, Y.L., Nguyen, T., Van Reyk, D., Saad, S., and Oliver, B.G. (2018b). Modulation of neural regulators of energy homeostasis, and of inflammation, in the pups of mice exposed to e-cigarettes. Neurosci. Lett. *684*, 61–66. https://doi.org/10.1016/j.neulet.2018.07.001.

Chen, R., Wu, X., Jiang, L., and Zhang, Y. (2017). Single-cell RNA-seq reveals hypothalamic cell diversity. Cell Rep. *18*, 3227–3241. https://doi.org/10.1016/j.celrep.2017.03.004.

Church, J.S., Chace-Donahue, F., Blum, J.L., Ratner, J.R., Zelikoff, J.T., and Schwartzer, J.J. (2020). Neuroinflammatory and behavioral outcomes measured in adult offspring of mice exposed prenatally to e-cigarette aerosols. Environ. Health Perspect. *128*, 047006. https://doi.org/10.1289/ehp6067.

Corces, M.R., Buenrostro, J.D., Wu, B., Greenside, P.G., Chan, S.M., Koenig, J.L., Snyder, M.P., Pritchard, J.K., Kundaje, A., Greenleaf, W.J., et al. (2016). Lineage-specific and single-cell chromatin accessibility charts human hematopoiesis and leukemia evolution. Nat. Genet. *48*, 1193–1203. https://doi.org/10.1038/ng.3646.

Cserép, C., Pósfai, B., Lénárt, N., Fekete, R., László, Z.I., Lele, Z., Orsolits, B., Molnár, G., Heindl, S., Schwarcz, A.D., et al. (2020). Microglia monitor and protect neuronal function through specialized somatic purinergic junctions. Science *367*, 528–537. https://doi.org/10.1126/science.aax6752.

Dwyer, J.B., Broide, R.S., and Leslie, F.M. (2008). Nicotine and brain development. Birth Defects Res. C Embryo Today *84*, 30–44. https://doi.org/10.1002/bdrc.20118.

Dwyer, J.B., Mcquown, S.C., and Leslie, F.M. (2009). The dynamic effects of nicotine on the developing brain. Pharmacol. Ther. *122*, 125–139. https://doi.org/10.1016/j.pharmthera.2009.02.003.

El Marroun, H., Schmidt, M.N., Franken, I.H.A., Jaddoe, V.W.V., Hofman, A., Van Der Lugt, A., Verhulst, F.C., Tiemeier, H., and White, T. (2014). Prenatal tobacco exposure and brain morphology: a prospective study in young children. Neuropsychopharmacology *39*, 792–800. https://doi.org/10.1038/npp.2013.273.

Espinoza-Derout, J., Hasan, K.M., Shao, X.M., Jordan, M.C., Sims, C., Lee, D.L., Sinha, S., Simmons, Z., Mtume, N., Liu, Y., et al. (2019). Chronic intermittent electronic cigarette exposure induces cardiac dysfunction and atherosclerosis in apolipoprotein-E knockout mice. Am. J. Physiol. Heart Circ. Physiol. *317*, H445–H459. https://doi.org/10.1152/ajpheart.00738.2018.

Fan, X., Fu, Y., Zhou, X., Sun, L., Yang, M., Wang, M., Chen, R., Wu, Q., Yong, J., Dong, J., et al. (2020). Single-cell transcriptome analysis reveals cell lineage specification in temporal-spatial patterns in human cortical development. Sci. Adv. *6*, eaaz2978. https://doi.org/10.1126/sciadv.aaz2978.

Faustino, J.V., Wang, X., Johnson, C.E., Klibanov, A., Derugin, N., Wendland, M.F., and Vexler, Z.S. (2011). Microglial cells contribute to endogenous brain defenses after acute neonatal focal stroke. J. Neurosci. *31*, 12992–13001. https://doi.org/10.1523/jneurosci.2102-11.2011.

Fletcher, R.B., Das, D., Gadye, L., Street, K.N., Baudhuin, A., Wagner, A., Cole, M.B., Flores, Q., Choi, Y.G., Yosef, N., et al. (2017). Deconstructing olfactory stem cell trajectories at single-cell resolution. Cell Stem Cell *20*, 817–830.e8. https://doi.org/10.1016/j.stem.2017.04.003.

Greenberg, M.E., Ziff, E.B., and Greene, L.A. (1986). Stimulation of neuronal acetylcholine receptors induces rapid gene transcription. Science *234*, 80–83. https://doi.org/10.1126/science.3749894.

Guan, Y.-Z., Jin, X.-D., Guan, L.-X., Yan, H.-C., Wang, P., Gong, Z., Li, S.-J., Cao, X., Xing, Y.-L., and Gao, T.-M. (2015). Nicotine inhibits microglial proliferation and is neuroprotective in global ischemia rats. Mol. Neurobiol. *51*, 1480–1488. https://doi.org/10.1007/s12035-014-8825-3.

Hellstrom-Lindahl, E., Gorbounova, O., Seiger, A., Mousavi, M., and Nordberg, A. (1998). Regional distribution of nicotinic receptors during prenatal development of human brain and spinal cord. Brain Res. Dev. Brain Res. *108*, 147–160. https://doi.org/10.1016/s0165-3806(98)00046-7.

Henrich, K.O., Bauer, T., Schulte, J., Ehemann, V., Deubzer, H., Gogolin, S., Muth, D., Fischer, M., Benner, A., Konig, R., et al. (2011). CAMTA1, a 1p36 tumor suppressor candidate, inhibits growth and activates differentiation programs in neuroblastoma cells. Cancer Res. *71*, 3142–3151. https://doi.org/10.1158/0008-5472.can-10-3014.

Hosseinzadeh, A., Thompson, P.R., Segal, B.H., and Urban, C.F. (2016). Nicotine induces neutrophil extracellular traps. J. Leukoc. Biol. *100*, 1105–1112. https://doi.org/10.1189/jlb.3ab0815-379rr.

Huang, L., Ma, Q., Li, Y., Li, B., and Zhang, L. (2018). Inhibition of microRNA-210 suppresses pro-inflammatory response and reduces acute brain injury of ischemic stroke in mice. Exp. Neurol. *300*, 41–50. https://doi.org/10.1016/j.expneurol.2017.10.024.

Iannaccone, P.M., and Jacob, H.J. (2009). Rats! (The Company of Biologists Limited).

Jin, W.-N., Shi, S.X.-Y., Li, Z., Li, M., Wood, K., Gonzales, R.J., and Liu, Q. (2017). Depletion of microglia exacerbates postischemic inflammation and brain injury. J. Cereb. Blood Flow Metab. *37*, 2224–2236. https://doi.org/10.1177/0271678x17694185.

Lacy, R.T., Brown, R.W., Morgan, A.J., Mactutus, C.F., and Harrod, S.B. (2016). Intravenous prenatal nicotine exposure alters METH-induced hyperactivity, conditioned hyperactivity, and BDNF in adult rat offspring. Dev. Neurosci. *38*, 171–185. https://doi.org/10.1159/000446563.

Lake, B.B., Ai, R., Kaeser, G.E., Salathia, N.S., Yung, Y.C., Liu, R., Wildberg, A., Gao, D., Fung, H.-L., Chen, S., et al. (2016). Neuronal subtypes and diversity revealed by single-nucleus RNA sequencing of the human brain. Science *352*, 1586–1590. https://doi.org/10.1126/science.aaf1204.

Lake, B.B., Chen, S., Sos, B.C., Fan, J., Kaeser, G.E., Yung, Y.C., Duong, T.E., Gao, D., Chun, J., Kharchenko, P.V., and Zhang, K. (2018). Integrative single-cell analysis of transcriptional and epigenetic states in the human adult brain. Nat. Biotechnol. *36*, 70–80. https://doi.org/10.1038/nbt.4038.

Lauterstein, D., Tijerina, P., Corbett, K., Akgol Oksuz, B., Shen, S., Gordon, T., Klein, C., and Zelikoff, J. (2016). Frontal cortex transcriptome analysis of mice exposed to electronic cigarettes during early life stages. Int. J. Environ. Res. Public Health *13*, 417. https://doi.org/10.3390/ijerph13040417.

Lee, H., Chung, S., and Noh, J. (2016). Maternal nicotine exposure during late gestation and lactation increases anxiety-like and impulsive decision-making behavior in adolescent offspring of rat. Toxicol. Res. *32*, 275–280. https://doi.org/10.5487/tr.2016.32.4.275.

Lee, H., Park, J.-R., Yang, J., Kim, E., Hong, S.-H., Woo, H.-M., Ryu, S.-M., Cho, S.-J., Park, S.-M., and Yang, S.-R. (2014). Nicotine inhibits the proliferation by upregulation of nitric oxide and increased HDAC1 in mouse neural stem cells. In Vitro Cell. Dev. Biol. Anim. *50*, 731–739. https://doi.org/10.1007/s11626-014-9763-0.

Lenz, K.M., and Nelson, L.H. (2018). Microglia and beyond: innate immune cells as regulators of brain development and behavioral function. Front. Immunol. *9*, 698. https://doi.org/10.3389/fimmu.2018.00698.

Li, Y., Huang, L., Ma, Q., Concepcion, K., Song, M., Zhang, P., Fu, Y., Xiao, D., and Zhang, L. (2018). Repression of the glucocorticoid receptor aggravates acute ischemic brain injuries in adult mice. Int. J. Mol. Sci. *19*, 2428. https://doi.org/10.3390/ijms19082428.

Li, Y., Ma, Q., Dasgupta, C., Halavi, S., Hartman, R.E., Xiao, D., and Zhang, L. (2017). Inhibition of DNA methylation in the developing rat brain disrupts sexually dimorphic neurobehavioral phenotypes in adulthood. Mol. Neurobiol. *54*, 3988–3999. https://doi.org/10.1007/s12035-016-9957-4.

Li, Y., Xiao, D., Dasgupta, C., Xiong, F., Tong, W., Yang, S., and Zhang, L. (2012). Perinatal nicotine exposure increases vulnerability of hypoxic–ischemic brain injury in neonatal rats: role of angiotensin II receptors. Stroke *43*, 2483–2490. https://doi.org/10.1161/strokeaha.112.664698.

Li, Y., Xiao, D., Yang, S., and Zhang, L. (2013). Promoter methylation represses AT2R gene and increases brain hypoxic–ischemic injury in neonatal rats. Neurobiol. Dis. *60*, 32–38. https://doi.org/10.1016/j.nbd.2013.08.011.

Lopez, A.A., Hiler, M.M., Soule, E.K., Ramôa, C.P., Karaoghlanian, N.V., Lipato, T., Breland, A.B., Shihadeh, A.L., and Eissenberg, T. (2016). Effects of electronic cigarette liquid nicotine concentration on plasma nicotine and puff topography in tobacco cigarette smokers: a preliminary report. Nicotine Tob. Res. *18*, 720–723. https://doi.org/10.1093/ntr/ntv182.

Luo, C., Keown, C.L., Kurihara, L., Zhou, J., He, Y., Li, J., Castanon, R., Lucero, J., Nery, J.R.,

Sandoval, J.P., et al. (2017). Single-cell methylomes identify neuronal subtypes and regulatory elements in mammalian cortex. Science *357*, 600–604. https://doi.org/10.1126/science.aan3351.

Maggi, L., Le Magueresse, C., Changeux, J.-P., and Cherubini, E. (2003). Nicotine activates immature "silent" connections in the developing hippocampus. Proc. Natl. Acad. Sci. USA *100*, 2059–2064. https://doi.org/10.1073/pnas.0437947100.

Mathys, H., Davila-Velderrain, J., Peng, Z., Gao, F., Mohammadi, S., Young, J.Z., Menon, M., He, L., Abdurrob, F., Jiang, X., et al. (2019). Single-cell transcriptomic analysis of Alzheimer's disease. Nature *570*, 332–337. https://doi.org/10.1038/s41586-019-1195-2.

McCubbin, A., Fallin-Bennett, A., Barnett, J., and Ashford, K. (2017). Perceptions and use of electronic cigarettes in pregnancy. Health Educ. Res. *32*, 22–32. https://doi.org/10.1093/her/cyw059.

McKay, B.E., Placzek, A.N., and Dani, J.A. (2007). Regulation of synaptic transmission and plasticity by neuronal nicotinic acetylcholine receptors. Biochem. Pharmacol. *74*, 1120–1133. https://doi.org/10.1016/j.bcp.2007.07.001.

Mittleman, B.B., Castellanos, F.X., Jacobsen, L.K., Rapoport, J.L., Swedo, S.E., and Shearer, G.M. (1997). Cerebrospinal fluid cytokines in pediatric neuropsychiatric disease. J. Immunol. *159*, 2994–2999.

Mognol, G.P., Carneiro, F.R.G., Robbs, B.K., Faget, D.V., and Viola, J.P.B. (2016). Cell cycle and apoptosis regulation by NFAT transcription factors: new roles for an old player. Cell Death Dis. *7*, e2199. https://doi.org/10.1038/cddis.2016.97.

Muhammad, A., Mychasiuk, R., Nakahashi, A., Hossain, S.R., Gibb, R., and Kolb, B. (2012). Prenatal nicotine exposure alters neuroanatomical organization of the developing brain. Synapse *66*, 950–954. https://doi.org/10.1002/syn.21589.

Newman, M.B., Shytle, R.D., and Sanberg, P.R. (1999). Locomotor behavioral effects of prenatal and postnatal nicotine exposure in rat offspring. Behav. Pharmacol. *10*, 699–706. https://doi.org/10.1097/00008877-199911000-00017.

Noda, M., and Kobayashi, A. (2017). Nicotine inhibits activation of microglial proton currents via interactions with α7 acetylcholine receptors. J. Physiol. Sci. *67*, 235–245. https://doi.org/10.1007/s12576-016-0460-5.

Papadimitriou, C.H., Raghavan, P., Tamaki, H., and Vempala, S. (2000). Latent semantic indexing: a probabilistic analysis. J. Comput. Syst. Sci. *61*, 217–235. https://doi.org/10.1006/jcss.2000.1711.

Pinheiro, C., Moura, E., Manhães, A., Fraga, M., Claudio-Neto, S., Younes-Rapozo, V., Santos-Silva, A., Lotufo, B., Oliveira, E., and Lisboa, P. (2015). Maternal nicotine exposure during lactation alters food preference, anxiety-like behavior and the brain dopaminergic reward system in the adult rat offspring. Physiol. Behav. *149*, 131–141. https://doi.org/10.1016/j.physbeh.2015.05.040.

Polioudakis, D., De La Torre-Ubieta, L., Langerman, J., Elkins, A.G., Shi, X., Stein, J.L., Vuong, C.K., Nichterwitz, S., Gevorgian, M., Opland, C.K., et al. (2019). A single-cell transcriptomic atlas of human neocortical development during mid-gestation. Neuron *103*, 785–801.e8. https://doi.org/10.1016/j.neuron.2019.06.011.

Preissl, S., Fang, R., Huang, H., Zhao, Y., Raviram, R., Gorkin, D.U., Zhang, Y., Sos, B.C., Afzal, V., Dickel, D.E., et al. (2018). Single-nucleus analysis of accessible chromatin in developing mouse forebrain reveals cell-type-specific transcriptional regulation. Nat. Neurosci. *21*, 432–439. https://doi.org/10.1038/s41593-018-0079-3.

Rosenberg, A.B., Roco, C.M., Muscat, R.A., Kuchina, A., Sample, P., Yao, Z., Graybuck, L.T., Peeler, D.J., Mukherjee, S., Chen, W., et al. (2018). Single-cell profiling of the developing mouse brain and spinal cord with split-pool barcoding. Science *360*, 176–182. https://doi.org/10.1126/science.aam8999.

Roy, T.S., Seidler, F.J., and Slotkin, T.A. (2002). Prenatal nicotine exposure evokes alterations of cell structure in hippocampus and somatosensory cortex. J. Pharmacol. Exp. Therapeut. *300*, 124–133. https://doi.org/10.1124/jpet.300.1.124.

Ruszkiewicz, J.A., Zhang, Z., Gonçalves, F.M., Tizabi, Y., Zelikoff, J.T., and Aschner, M. (2020). Neurotoxicity of e-cigarettes. Food Chem. Toxicol. *138*, 111245. https://doi.org/10.1016/j.fct.2020.111245.

Sailer, S., Sebastiani, G., Andreu-Férnández, V., and García-Algar, O. (2019). Impact of nicotine replacement and electronic nicotine delivery systems on fetal brain development. Int. J. Environ. Res. Publ. Health *16*, 5113. https://doi.org/10.3390/ijerph16245113.

Schafer, D.P., and Stevens, B. (2015). Microglia function in central nervous system development and plasticity. Cold Spring Harbor Perspect. Biol. *7*, a020545. https://doi.org/10.1101/cshperspect.a020545.

Schmidt, S. (2020). E-cigarette aerosols and the brain: behavioral and neuroinflammatory changes in prenatally exposed adult mice. Environ. Health Perspect. *128*, 104005. https://doi.org/10.1289/ehp7315.

Shao, X.M., Lopez, B., Nathan, D., Wilson, J., Bankole, E., Tumoyan, H., Munoz, A., Espinoza-Derout, J., Hasan, K.M., Chang, S., et al. (2019). A mouse model for chronic intermittent electronic cigarette exposure exhibits nicotine pharmacokinetics resembling human vapers. J. Neurosci. Methods *326*, 108376. https://doi.org/10.1016/j.jneumeth.2019.108376.

Sifat, A.E., Nozohouri, S., Villalba, H., Al Shoyaib, A., Vaidya, B., Karamyan, V.T., and Abbruscato, T. (2020). Prenatal electronic cigarette exposure decreases brain glucose utilization and worsens outcome in offspring hypoxic–ischemic brain injury. J. Neurochem. *153*, 63–79. https://doi.org/10.1111/jnc.14947.

Silva, C.P., Horton, W.J., Caruso, M.J., Sebastian, A., Klein, L.C., Albert, I., and Kamens, H.M. (2018). The influence of adolescent nicotine exposure on ethanol intake and brain gene expression. PLoS One *13*, e0198935. https://doi.org/10.1371/journal.pone.0198935.

Singh, S., Gupta, A., Zech, M., Sigafoos, A.N., Clark, K.J., Dincer, Y., Wagner, M., Humberson, J.B., Green, S., Van Gassen, K., et al. (2020). De novo variants of NR4A2 are associated with neurodevelopmental disorder and epilepsy. Genet. Med. *22*, 1413–1417. https://doi.org/10.1038/s41436-020-0815-4.

Sinha, S., Satpathy, A.T., Zhou, W., Ji, H., Stratton, J.A., Jaffer, A., Bahlis, N., Morrissy, S., and Biernaskie, J.A. (2021). Profiling chromatin accessibility at single-cell resolution. Dev. Reprod. Biol. *19*, 172–190. https://doi.org/10.1016/j.gpb.2020.06.010.

Siniscalco, D., Schultz, S., Brigida, A., and Antonucci, N. (2018). Inflammation and neuro-immune dysregulations in autism spectrum disorders. Pharmaceuticals *11*, 56. https://doi.org/10.3390/ph11020056.

Smajić, S., Prada-Medina, C.A., Landoulsi, Z., Dietrich, C., Jarazo, J., Henck, J., Balachandran, S., Pachchek, S., Morris, C.M., Antony, P., et al. (2020). Single-cell sequencing of the human midbrain reveals glial activation and a neuronal state specific to Parkinson's disease. Preprint at medRxiv. https://doi.org/10.1101/2020.09.28.20202812.

Smith, A., Dwoskin, L., and Pauly, J. (2010). Early exposure to nicotine during critical periods of brain development: mechanisms and consequences. J. Pediatr. Biochem. *1*, 125–141. https://doi.org/10.1055/s-0036-1586367.

St. Helen, G., Havel, C., Dempsey, D.A., Jacob, P., Iii, and Benowitz, N.L. (2016). Nicotine delivery, retention and pharmacokinetics from various electronic cigarettes. Addiction *111*, 535–544. https://doi.org/10.1111/add.13183.

Street, K., Risso, D., Fletcher, R.B., Das, D., Ngai, J., Yosef, N., Purdom, E., and Dudoit, S. (2018). Slingshot: cell lineage and pseudotime inference for single-cell transcriptomics. BMC Genom. *19*, 477. https://doi.org/10.1186/s12864-018-4772-0.

Stuart, T., Srivastava, A., Lareau, C., and Satija, R. (2020). Multimodal single-cell chromatin analysis with Signac. Preprint at bioRxiv. https://doi.org/10.1101/2020.11.09.373613.

Szalay, G., Martinecz, B., Lénárt, N., Környei, Z., Orsolits, B., Judák, L., Császár, E., Fekete, R., West, B.L., Katona, G., et al. (2016). Microglia protect against brain injury and their selective elimination dysregulates neuronal network activity after stroke. Nat. Commun. *7*, 11499. https://doi.org/10.1038/ncomms11499.

Tan, G., and Lenhard, B. (2016). TFBSTools: an R/bioconductor package for transcription factor binding site analysis. Genome Anal. *32*, 1555–1556. https://doi.org/10.1093/bioinformatics/btw024.

Tirosh, I., Izar, B., Prakadan, S.M., Wadsworth, M.H., Treacy, D., Trombetta, J.J., Rotem, A., Rodman, C., Lian, C., Murphy, G., et al. (2016). Dissecting the multicellular ecosystem of metastatic melanoma by single-cell RNA-seq. Science *352*, 189–196. https://doi.org/10.1126/science.aad0501.

Visser, W.F., Klerx, W.N., Cremers, H.W.J.M., Ramlal, R., Schwillens, P.L., and Talhout, R. (2019). The health risks of electronic cigarette use to

bystanders. Int. J. Environ. Res. Publ. Health *16*, 1525. https://doi.org/10.3390/ijerph16091525.

Vuong-Brender, T.T., Flynn, S.M., and De Bono, M. (2020). Transcriptional control of calmodulin by CAMTA regulates neural excitability. Preprint at bioRxiv. https://doi.org/10.1101/2020.09.14.296137.

Wakschlag, L.S., Pickett, K.E., Cook, E., Jr., Benowitz, N.L., and Leventhal, B.L. (2002). Maternal smoking during pregnancy and severe antisocial behavior in offspring: a review. Am. J. Publ. Health *92*, 966–974. https://doi.org/10.2105/ajph.92.6.966.

Whittington, J.R., Simmons, P.M., Phillips, A.M., Gammill, S.K., Cen, R., Magann, E.F., and Cardenas, V.M. (2018). The use of electronic cigarettes in pregnancy: a review of the literature. Obstet. Gynecol. Surv. *73*, 544–549. https://doi.org/10.1097/ogx.0000000000000595.

Ximerakis, M., Lipnick, S.L., Innes, B.T., Simmons, S.K., Adiconis, X., Dionne, D., Mayweather, B.A., Nguyen, L., Niziolek, Z., Ozek, C., et al. (2019a). Single-cell transcriptomic profiling of the aging mouse brain. Nat. Neurosci. *22*, 1696–1708. https://doi.org/10.1038/s41593-019-0491-3.

Ximerakis, M., Lipnick, S.L., Innes, B.T., Simmons, S.K., Adiconis, X., Dionne, D., Mayweather, B.A., Nguyen, L., Niziolek, Z., Ozek, C., et al. (2019b). Single-cell transcriptomic profiling of the aging mouse brain. Nat. Neurosci. *22*, 1696–1708. https://doi.org/10.1038/s41593-019-0491-3.

Zamanighomi, M., Lin, Z., Daley, T., Chen, X., Duren, Z., Schep, A., Greenleaf, W.J., and Wong, W.H. (2018). Unsupervised clustering and epigenetic classification of single cells. Nat. Commun. *9*, 2410. https://doi.org/10.1038/s41467-018-04629-3.

Zelikoff, J.T., Parmalee, N.L., Corbett, K., Gordon, T., Klein, C.B., and Aschner, M. (2018). Microglia activation and gene expression alteration of neurotrophins in the hippocampus following early-life exposure to e-cigarette aerosols in a murine model. Toxicol. Sci. *162*, 276–286. https://doi.org/10.1093/toxsci/kfx257.

Zhang, C., Fan, S.J., Sun, A.B., Liu, Z.Z., and Liu, L. (2019). Prenatal nicotine exposure induces depression-like behavior in adolescent female rats via modulating neurosteroid in the hippocampus. Mol. Med. Rep. *19*, 4185–4194. https://doi.org/10.3892/mmr.2019.10105.

Zhang, L., Spencer, T.J., Biederman, J., and Bhide, P.G. (2018). Attention and working memory deficits in a perinatal nicotine exposure mouse model. PLoS One *13*, e0198064. https://doi.org/10.1371/journal.pone.0198064.

Zhu, C., Yu, M., Huang, H., Juric, I., Abnousi, A., Hu, R., Lucero, J., Behrens, M.M., Hu, M., and Ren, B. (2019). An ultra high-throughput method for single-cell joint analysis of open chromatin and transcriptome. Nat. Struct. Mol. Biol. *26*, 1063–1070. https://doi.org/10.1038/s41594-019-0323-x.

Zoli, M., Le Novere, N., Hill, J.A., and Changeux, J.-P. (1995). Developmental regulation of nicotinic ACh receptor subunit mRNAs in the rat central and peripheral nervous systems. J. Neurosci. *15*, 1912–1939. https://doi.org/10.1523/jneurosci.15-03-01912.1995.

STAR★METHODS

KEY RESOURCES TABLE

REAGENT or RESOURCE	SOURCE	IDENTIFIER
Biological Samples		
Pregnant Sprague-Dawley rats	Charles River Laboratory (Portage, MI)	RRID:RGD_10395233
Critical Commercial Assays		
BluePlus Cig (2.4% nicotine)	blu.com	NA
10x Genomics Chromium Next GEM Single Cell 3' Reagent Kits v3.1.	10x Genomics	1000128
10x Genomics Chromium Single Cell ATAC Reagent Kits v1.1	10x Genomics	1000164
KAPA library quantification	Roche	KK4873
Protector RNase inhibitor	Sigma Aldrich	03335402001
PBS	Gibco	10010-023
Nuclei PURE lysis buffer	Sigma Aldrich	L9286-180ML
Nuclei PURE sucrose cushion solution	Sigma Aldrich	S9058-120ML
Nuclei PURE storage buffer	Sigma Aldrich	S9183-30ML
Isoflurane	PubChem	3763
IBA1 antibody	Cell Signaling Technology	Cat# 17198S; RRID: AB_2820254
Secondary antibody	EMD Millipore	Cat# 401393; RRID: AB_437797
Deposited Data		
All sequencing fastq files generated in this project	Gene Expression Omnibus	GEO:GSE185538
Software and Algorithms		
CellRanger	10x Genomics	V3.1.0
CellRanger-atac	10x Genomics	V1.2.0
Seurat	satijalab.org/Seurat/	V3.0
Signac	satijalab.org/signac/	V1.4.0
rGADEM	Droit et al., 2021	V2.40.0
TFBSTools	Tan G, Lenhard B. 2016	V1.30.0
JASPAR database	jaspar.genereg.net	V2020
Slingshot	Street K et al., 2018	V1.2.0
ShinyGo	bioinformatics.sdstate.edu/go	V0.66
Fastqc	Andrew S, 2010	V0.11.4
Other		
QuantStudio 7 Flex Real-Time PCR System	Applied Biosystems	Cat No.44-856-98
NextSeq 550 Sequencing System	Illumina	https://www.illumina.com/systems/sequencing-platforms/nextseq.html
HiSeq 4000 System	Illumina	https://www.illumina.com/systems/sequencing-platforms/hiseq.html

RESOURCE AVAILABILITY

Lead contact

Further information and requests for resources and reagents should be directed to and will be fulfilled by the lead contact, Charles Wang (chwang@llu.edu).

Material availability

This study did not generate new unique reagents and animal strain.

Data and code availability

- The sequencing data generated in this study are deposited to the NCBI GEO (accession number: GSE185538) and are publicly available.
- We used many publicly available algorithms and packages for the rat snRNA-seq and snATAC-seq mapping, genome annotation, differential analysis, lineage predication, *etc.*, which were cited properly in the manuscript. This paper did not produce original code.
- Any additional information required for reanalyzing the reported data is available from the lead contact upon request.

EXPERIMENTAL MODEL AND SUBJECT DETAILS

All animal experiments involving animal care, surgery, and sample preparation were approved by the Institutional Animal Care and Use Committee of Loma Linda University and followed the guidelines by the National Institutes of Health Guide for the Care and Use of Laboratory Animals. All efforts were made to minimize animal suffering and the number of animals used. Pregnant Sprague-Dawley rats were purchased from Charles River Laboratories (Portage, MI) and were housed under controlled temperature (22°C) and photoperiod (12-h light and 12-h dark cycle) with food and water *ad libitum*.

METHOD DETAILS

Prenatal e-cigarette exposure

We developed a chronic intermittent e-cigarette (CIEC) exposure model in pregnant rats which was slightly modified from previous studies (Espinoza-Derout et al., 2019; Shao et al., 2019). The e-cigarette rodent exposure system was manufactured by AutoMate Scientific, Inc (Berkeley, CA). This system contains air pressure and flow rate control as well as hardware and software that allow experimenters to control the timing, duration, and times/day for CIEC aerosol generation/exposure and attaches a free-moving rodent exposure chamber. Briefly, the pregnant Sprague-Dawley rats were randomly divided into two groups: the first group was exposed to e-cigarette aerosol; the 2nd group was exposed to air in the same type of chamber. Commercial (BluPlus Cig) e-cigarettes (2.4% nicotine) were used for this project to reflect what real-world e-cigarette users are experiencing. In order to mimic the phenomenon of chronic intermittent e-cigarette exposure in human vaporizers, we optimized the system to deliver e-cigarette aerosol with a puff duration of 4 s, 3 puffs in an inter-puff interval of 30 s per vaping episode, and one episode per 1 h in the dark phase of 12 h each day, which generates similar nicotine blood pharmacokinetics in the pregnant rats to those observed in human e-cigarette users (Lopez et al., 2016; St. Helen et al., 2016). The dams were exposed to e-cigarette for a total of 17 days from gestational day 4 (E4) to E20. The rationale for starting on E4 is that this is the period just before embryo implantation on the uterine wall in rat.

Brain tissue dissection, single nucleus isolation, and capture

Four male and four female P7 neonatal rats from either prenatal e-cigarette exposure or control were selected for this experiment (2 pups per dam). Briefly, rat pups or adult rats were euthanized by decapitation under deep isoflurane anesthesia. The prefrontal cortex and hippocampus were isolated on ice from the whole brain as previously described (Li et al., 2017). In each sample, four prefrontal cortexes and hippocampi were pooled for single nucleus isolation. All steps were carried out in the cold and the environment was sprayed with RNase inhibitor. We chose prefrontal cortex and hippocampus because 1) these regions are involved in higher-order brain functions such as cognition, learning, memory, and generation of motor commands; 2) these regions are plastic and vulnerable to a variety of stimuli. For single-nucleus RNA-seq (snRNA-seq), single nuclei were isolated following 10x Genomics protocol "Isolation of Nuclei for Single Cell RNA Sequencing" (CG000124). snRNA-seq library preparation was performed following the manual for the 10x Genomics Chromium Next GEM Single Cell 3' Reagent Kits v3.1. Briefly, based on the cell suspension volume calculator table supplied by 10X Genomics, 10,000 nuclei and barcode-beads as well as RT reagents were loaded into the Chromium Controller to generate single nucleus Gel Bead-in-Emulsions (GEMs). cDNAs were generated after GEM-RT incubation at 53°C for 45 min and 85°C for 5 min. cDNA amplification was performed for 11 PCR cycles following GEM cleanup. After size selection with SPRIselect Reagent, cDNA was incubated for fragmentation, end repair & A-tailing, adapter ligation,

and finally library amplification. For single-nucleus ATAC-seq (snATAC-seq), single nuclei were isolated following the 10x Genomics protocol "Nuclei isolation from Mouse Brain Tissue for Single Cell ATAC sequencing" (CG000212). snATAC-seq library preparation was performed following the manual for the Chromium Single Cell ATAC Reagent Kits v1.1. Briefly, suspensions of single nuclei were first incubated in a transposition mix at 37°C for 60 min. Based on the nucleus concentration guidelines and calculation formula from 10X Genomics, 10,000 nuclei were loaded into the Chromium Controller to generate single nucleus GEMs & barcoding. After post GEM cleanup, Illumina P7 indices and a sample index were added for final library construction.

Library sequencing

The final library was quantified using the KAPA library quantification kit for Illumina platforms (KK4873, Roche, Indianapolis, IN). For gene expression libraries, sequencing was performed on a NextSeq 550 using high output kit or a HiSeq 4000 using SBS reagents (Illumina, Inc., San Diego, CA), with the following settings: Read 1 28 cycles, I7 index 8 cycles, Read 2 91 cycles. FASTQ files were generated from the Illumina sequencer Base Call files (bcl files) using 10x Genomics CellRanger mkfastq (version 3.1.0) software. Gene expression counts were generated by aligning reads to the Rnor 6.0 genome (NCBI: GCA_000001895.4) using CellRanger count software (v.3.1.0) (10x Genomics). After quality trimming, all fastq files belonging to a single GEM well but from different sequencing runs were pooled and counted together. As nuclear transcripts were unspliced, only reads mapped to pre-mRNA were counted. For snATAC-seq libraries, sequencing was performed on an Illumina NextSeq 550 using high output kit (150 cycles) (Illumina, Inc., San Diego, CA), with the following settings: Read 1 50 cycles, I7 index 8 cycles, I5 index 16 cycles, Read 2 50 cycles. FASTQ files were generated from bcl files using 10x Genomics CellRanger-atac mkfastq (version 1.2.0) software.

snRNA-seq data analysis

Cells with fewer than 200 genes, fewer than 1000 transcripts (UMIs), or those with more than 8.5% mitochondrial gene transcripts were filtered out. The four datasets (female control: 10,356 nuclei, female E-Cig: 9,403 nuclei, male control: 4,878 nuclei, and male E-Cig: 4,680 nuclei) were merged to generate a single dataset for downstream data analysis. We used Seurat (version 3.0) to perform dimension reduction and graph-based unbiased clustering (Butler et al., 2018) (Butler et al., 2018). In brief, we identified the top 2000 most highly variable genes in each dataset and used these to compute principal components. The top 30 variables were used for either UMAP (Uniform Manifold Approximation and Projection) or t-SNE (t-distributed stochastic neighbor embedding) dimension reduction. Molecularly distinct clusters were identified using the FindClusters function with the original Louvain algorithm. This allowed us to identify 21 cell types in the combined dataset. Cluster marker genes were identified using the FindConservedMarkers function, and those marker genes were cross-referenced with known cell markers to identify cell types. To further resolve cell subtypes, target cell clusters were extracted from the combined dataset using the Subset function and cluster ID. The subset was subjected to a new round of normalization, dimension reduction, and clustering to identify subtypes. Differentially expressed genes (DEGs) between prenatal e-cigarette exposure and control groups were determined using the FindMarkers function. All Seurat-generated clusters containing >50 cells were included. DEGs were reported as FDR<0.2 and fold change >1.25. Conserved cell type markers were determined by differential gene expression analysis of cells in each cluster against the remaining cells of the whole dataset using FindConservedMarkers function. Significantly overexpressed genes were defined by the Wilcoxon rank-sum test in Seurat (version 3.0) with FDR< 0.01 and fold change of >1.25.

snATAC-seq data analysis

Chromatin accessibility counts were generated by mapping reads to Rnor 6.0 and counting the number of reads from individual cells that overlaid the union peaks using CellRanger-atac count (version 1.2.0). We used Signac (Stuart et al., 2020) to analyze the snATAC-seq peak count data generated by 10x CellRanger-atac count. Peak counts from four datasets (female control, femalee-cig, male control, and male e-cig) were merged from common peak regions for analysis. Low quality cells with fewer than 200 genes and TSS enrichment scores less than 2 were removed from the dataset. To reduce dimensions, term frequency and smoothed inverse document frequency (TF-IDF) were used as a weighting scheme to transform peak counts into binary data. Weighted data were reduced to 50 dimensions using the RunSVD function. The first SVD (singular value decomposition) component was identified as being strongly correlated with read depth; therefore, it was excluded from the subsequent UMAP projection. Differential

accessibility regions (DARs) between prenatal e-cigarette exposure and control were identified using the FindMarkers function with logistic regression. DNA regions were visualized using the CoveragePlot function.

To discover transcription factor binding motifs from the DARs, we performed motif analysis using the R package "rGADEM" (v 2.40.0) (Droit et al., 2021) and BSgenome.Rnorvegicus.UCSC.rn6. The Frequency matrix generated from "rGADEM" was used to compare the unknown sequence patterns with the transcription factor database ("JASPAR2020", downloaded from http://jaspar.genereg.net/), using the R package "TFBSTools" (Tan and Lenhard, 2016) (v 1.30.0).

snRNA-seq and snATAC-seq integration analysis

To examine the regulatory role of chromatin opening in gene expression, we combined the snATAC-seq data with the snRNA-seq data. In brief, we performed canonical correlation analysis (CCA) between snRNA-seq gene expression and snATAC-seq chromatin accessibility, using the FindTransferAnchors function. CCA captures the common variances between the two datasets and projects them into two-dimensional space as anchored cell pairs. Next, cell type labels from snRNA-seq were transferred to the scATAC-seq datasets using the TransferData function. For visualization, normalized gene expression values from snRNA-seq and chromatin accessibility from snATAC-seq were extracted across clusters and cells.

Cell lineage and neuron differentiation in pseudotime

We used the R package Slingshot (Fletcher et al., 2017) (https://github.com/kstreet13/slingshot, version 1.2.0) to reconstruct the pseudotime trajectory and to infer cell lineage from either snRNA-seq or snATAC-seq cell clusters. To order neurons based on snATAC data in pseudotime, we selected neuroblasts as the starting points and either inLGE cells (inhibitory neurons trajectory) or exL4 and exVII cells (excitatory neurons trajectory) as the endpoint, respectively. Cells on each trajectory were divided into ten quantiles according to their trajectory pseudotime calculated from Slingshot. DARs were determined between the starting points and the endpoints. The dynamic promoter accessibilities of those genes involved in neuron differentiation were visualized by row scaled DARs heatmaps over pseudotime.

Custom indexed reference genomes for rat single nucleus RNA-seq and ATAC-seq

Cellranger mkgtf tool was used to prepare a custom rat pre-mRNA gtf (General Transfer Format) from Rnor6.0.94.gtf (downloaded from http://ftp.ensembl.org/pub/release-104/gtf/rattus_norvegicus/), with attributes including protein coding, lincRNA, antisense, and all immunoglobulin genes that undergo somatic recombination. The Cellranger mkref tool was used to build an indexed rat pre-mRNA reference genome from the pre-mRNA gtf and rat Rnor6.0 genome (http://ftp.ensembl.org/pub/release-104/fasta/rattus_norvegicus/dna/). The Cellranger-atac mkref tool was used to prepare a rat single cell ATAC-seq reference package from Rnor6.0 genome, annotation gtf, and a transcription factor motif file downloaded from http://jaspar2018.genereg.net/downloads/.

Canonical pathway and molecular function analysis

Analyses of the gene networks, canonical, and bio-functional pathways were performed using the Ingenuity Pathway Analysis (IPA, Qiagen) and Gene Ontology Enrichment Analysis tools (ShinyGo v0.66, http://bioinformatics.sdstate.edu/go/). For IPA, the sets of all DEGs were input into the IPA database to discover canonical pathways regulated by e-cigarette exposure. We also applied the ShinyGO enrichment tool to the lists of DEGs and DAR linked genes to identify the molecular functions and biological processes that might be regulated by maternal e-cigarette exposure at the transcriptome and/or chromatin accessibility level.

Transient middle cerebral artery occlusion (tMCAO)

tMCAO was conducted on postnatal day 9 rat pups of both sexes as described previously (Huang et al., 2018; Li et al., 2018). Briefly, rat pups were anesthetized with isoflurane (4–5% for induction and 2% for maintenance) using a face mask. The left common carotid artery and external carotid artery were exposed through a midline neck incision. A 6-0 nylon monofilament coated with silicone rubber (Doccol) was introduced into the left internal carotid artery through the external carotid stump to occlude the origin of the middle cerebral artery and block blood flow to the striatum and cortex. After 3 h of occlusion, reperfusion was introduced by filament withdrawal, and the incision was sutured. During the whole procedure, the pup

body temperature was maintained at 37 ± 0.5°C. Sham-operated rat pups underwent a similar surgery but the filament was removed immediately after insertion (no occlusion, no reperfusion). No animal died during the MCAO procedure.

Measurement of infarct size

48 h after the MCAO treatment, rat pups were euthanized with isoflurane. Whole brain was isolated. Brain infarct size was evaluated by 2,3,5-triphenyltetrazolium chloride monohydrate (TTC) staining as previously described (Huang et al., 2018; Li et al., 2018). Briefly, coronal slices of the brain (2 mm thick) were cut and immersed in a pre-warmed, 2% solution of 2,3,5-triphenyltetrazolium chloride monohydrate (TTC) for 10 min at 37°C followed by fixation with 10% formaldehyde overnight. Both sides of each slice were photographed separately. The infarct area was analyzed by the ImageJ software (Version 1.40; National Institutes of Health, Bethesda, Maryland, MD, USA), summed for each brain, and expressed as a percentage of the whole brain.

Western blotting analysis

Brain samples were isolated from P9 rat pups of both sexes and were homogenized with a lysis buffer containing 150 mmol/L NaCl, 50 mmol/L Tris HCl, 10 mmol/L EDTA, 0.1% Tween 20, 1% Triton X-100, 0.1% β-mercaptoethanol, 0.1 mmol/L phenylmethylsulfonyl fluoride, 5 μg/mL leupeptin, and 5 μg/mL aprotinin, pH 7.4. Homogenates were centrifuged at 4°C for 15 min at 14,000 g. The supernatants were then collected, and protein concentrations were determined via a protein assay kit (Bio-Rad, Hercules, CA). Samples with equal amounts of protein (30 μg) were loaded onto 12% polyacrylamide gels with 0.1% sodium dodecyl sulfate in the running buffer and separated by sodium dodecyl sulfate polyacrylamide gel electrophoresis. Proteins were then transferred onto nitrocellulose membranes. Nonspecific binding sites were blocked for 3 to 4 h at room temperature in a Tris-buffered saline solution containing 5% non-fat dry milk. The membranes were probed with primary antibodies against IBA1 (1:1000, Cell Signaling Technology, Danvers, MA). After washing, membranes were incubated with secondary antibodies conjugated with horseradish peroxidase. Proteins were visualized with enhanced chemiluminescence reagents and blots were exposed to Hyperfilm. The results were analyzed with Kodak ID image analysis software. Band intensities were normalized to glyceraldehyde-3-phosphate dehydrogenase (GAPDH).

QUANTIFICATION AND STATISTICAL ANALYSIS

All data are presented as the Mean ± SD. In bulk RNA-seq, Western-blot, and ischemic injury experiments, five animals were used in each group. Cell proportion was calculated by combining the two subgroups (female and male) in each treatment group (e-cigarette and control), respectively. To compare the difference, p values were calculated from two-tailed Student's *t* test with a significance level of 95%. For single nucleus RNA-seq and ATAC-seq data, four animals were pooled in each group (female control, male control, female e-cigarette, and male e-cigarette). The differential expression or accessibility was determined by the non-parametric Wilcoxon rank-sum test as part of the Seurat package. Both the p values and the adjusted p values were reported in the single nucleus sequencing data.